Western Graduate&PostdoctoralStudies

Electronic Thesis and Dissertation Repository

7-30-2019 2:00 PM

Optimal Decentralized Coordination of Sources in Islanded and Grid-connected Microgrids

Mithun Mallick, *The University of Western Ontario*

© Mithun Mallick 2019

Follow this and additional works at: https://ir.lib.uwo.ca/etd

Part of the Power and Energy Commons

Abstract

Rising climate change concerns in recent years have instigated the emergence of sustainable sources to reduce dependence on high-emission, isolated bulk generation systems. The microgrid framework relies on integrating these distributed energy resources (DERs) to achieve regional energy independence that leads to a reliable and environment-friendly power grid. In this work, highly granular and decentralized coordination schemes are proposed that will enable fast computation of source dispatch set-points, thereby appropriately accounting for frequent changes in regional load-supply configuration of a microgrid. The mathematical models utilized in the study sufficiently represent the steady-state electrical interdependencies and feasibility limits in islanded or grid-connected operation modes. Applying alternating direction method of multipliers (ADMM) algorithm, the coordination process is transformed into a decentralized multi-agent problem involving minimal information exchange between subsystems. To overcome non-convexities typically present in optimization problem of microgrids, the two distinct convex relaxation techniques utilized are: 1) Linearization and 2) S-procedure. In separate coordination schemes, the former lends the advantage of extremely fast computation speed, while the latter exploits the hidden convexity in the decomposed coordination problem to deliver solutions with superior feasibility guarantee. Finally, the convergence, feasibility and scalability of the proposed coordination techniques are assessed with simulation studies performed on realistic microgrid parameters and several IEEE test systems.

Keywords: Microgrids, Computational Modelling, Steady-state, Decentralized Optimization, Convexity

Dedicated to my late father.

Summary for Lay Audience

Rising climate change concerns in recent years have instigated the emergence of sustainable energy sources to reduce dependence on high-emission, isolated bulk generation systems. The grid is being segmented into small regional blocks named microgrids that are ideally self-sufficient due to the incorporation of distributed generation systems known as DERs. The combination of these independent blocks is redefining the structure of the modern electrical grid, which is aptly named as smart grid. The much required paradigm shift from conventional unidirectional structure to a dynamic and autonomous grid has improved the reliability and resiliency of energy delivery manifold. As the technology allows for a widespread energy penetration from potentially every single household, challenges arise as to making the process of energy sharing economical, whilst sustaining the technical integrity of the grid. To this end, this work contributes a decentralized scheme for optimizing power-sharing among the participating energy supply systems (DERs) in the microgrids, so as to ultimately minimize the cost of energy consumption for the energy consumers. The applicability of an individual scheme from the offered variety in this work would depend on the characteristics of the system loads and logistic limitations. The coordination scheme is foreseen to work in tandem with transient control mechanisms that deals with initial oscillations and abrupt changes in system model between two instances of coordination shot. Therefore, the combined source control system will be robust and economically-efficient in facilitating the seamless operation of a microgrid and as a whole, the smart grid system.

Acknowlegements

First of all, I would like to thank my supervisor, Dr. Pirathayini Srikantha, for her guidance and support over the course of this degree. I have throughly enjoyed our stimulating discussions regarding research, academia and career. She has shown extraordinary patience and conviction in getting the best out of me, which in turn taught me the value of hardwork and perseverance in realizing one's ambitions. This extremely rewarding experience would not have been possible without her.

I would also like to thank the thesis examination committee members, Dr. Firouz Badrkhani Ajaei, Dr. Rajiv Varma and Dr. Jubayer Chowdhury for their time and constructive feedback.

Finally I would like to thank my wife, my mother and all my family members for their support during the times that I felt lost, being so far away from home. This is more for them, than for me.

Contents

List of Figures

List of Tables

List of Appendices

List of Acronyms

ADMM	Alternating Direction Method of Multipliers
BES	Battery Energy Storage
BFM	Branch Flow Model
DER	Distributed Energy Resources
DG	Distributed Generation
DQ	Direct Quadrature
DN	Distribution Network
ED	Economic Dispatch
GPS	Global Positioning System
IEEE	Institute of Electrical and Electronic Engineers
IoT	Internet-of-Things
OPF	Optimal Power Flow
PSD	Positive Semi-Definite
QCQP	Quadratically Constrained Quadratic Program
QP	Quadratic Program
SDP	Semi-definite Program
SOC	Second Order Cone
SOCP	Second Order Cone Program
SoC	State-of-Charge
VSC	Voltage Source Converter

Chapter 1

Introduction

The evolution of microgrid technology is enabling increased penetration of sustainable and distributed energy resources to reduce mankind's carbon footprint. Microgrids offer regional energy independence that can prevent perpetuation of outages and mitigate economic losses incurred due to grid interruptions [1]. Furthermore, the close proximity of sources to consumer loads can substantially decrease transmission and distribution losses [2]. Despite the rising prospects, a sustainable and economically-efficient operational framework for microgrids that can appropriately incentivize source deployment at consumer level remains an open research challenge.

The operational state of a microgrid can be classified into *stand-alone* and *grid-connected* mode. Several stand-alone microgrids with battery energy storage (BES) based source dispatch have been implemented to harness energy for remote localities, as a cost-effective alternative to establishing a grid-connection infrastructure [3]. However due to absence of grid inertia, such independent microgrids are susceptible to instabilities and inefficiencies caused by changes in load-supply characteristics in the network. This requires development of source dispatch techniques with short coordination time horizon, so that frequent source adjustments can be made to sustain efficient operation.

In grid-connected mode, the power demand in the microgrid is met partly by grid injection, while the rest of it is supplied by distributed energy resources (DERs). It is essentially an

1

active distribution network (DN) but with adequate distributed generation capacity to support loads for a certain or indefinite period of operation. Technological innovation and government subsidies have led to a remarkable drop in installation, maintenance and operational costs of distributed generation (DG) systems in the past decade. This combined with optimal power sharing schemes for on-site generations will facilitate peer-to-peer energy trading in DNs using technologies such as blockchain [4].

1.1 Literature Review

Due to climate change concerns and long-run economic benefits, microgrids have been the subject of much interest to power engineers. Several steady-state and transient control strategies have emerged over the years in order to streamline the microgrid technology [5]-[7] . As relevant to the thesis topic, the focus of this section is reviewing existing research on coordination techniques of distributed sources that ensues optimal steady-state operation of microgrids in islanded or grid-connected modes. Optimal power flow (OPF) problems for microgrids generally contain non-convexities that inhibit exact optimization. These need to be overcome through relaxations or mathematical manipulations to enable tractable analysis [8].

Existing source coordination techniques to optimize real power sharing in microgrids can be broadly classified into: *centralized* and *decentralized* schemes. In centralized coordination schemes, the computational burden of determining optimal set-points for the distributed sources fall on a central entity, which often rely on extensive communication with the subsystems (i.e. local buses). Sheer scale of information exchange and computational complexity of solving non-convex problems makes it impractical for centralized schemes to carry out online calculations with frequent system updates. Non-convexities in the OPF problems are mostly tackled using heuristic techniques or convex relaxations [9]-[12]. However, heuristic techniques do not guarantee optimality and relaxations might result in infeasible solutions. For example, reference [10] applies a second-order cone relaxation to a non-convex quadratic equality and mathematically proves that it yields feasible and optimal solution under limited bidirectional power flow in the distribution lines. This condition proves to be prohibitive for

active DNs with high injection from distributed sources and more so for islanded microgrids [11]. In reference [12], a traditional master-slave coordination approach is implemented where a dominant distributed generator (DG) acts like a slack bus to regulate the voltage whilst the other DGs participate in capacity based power sharing. The performance of this method being contingent on available capacity of the dominant DG does not fully utilize the potential benefits of the other DGs and causes reliability concerns, as the system will collapse if the dominant DG goes offline. Many centralized coordination schemes also relent to using forecast models of renewable generation and system loads for performing offline steady-state optimization over long time horizons[13, 14]. Such forecast models are associated with prediction errors [15]. Therefore, deviations in real-time operation from these forecasted values may lead to suboptimal operation .

In decentralized methods, dispatch set-point of a distributed source is determined by a local intelligent device, which may engage in communication with its decentralized counterparts in the network. Droop-based power sharing methods are very fast (timescale of milliseconds) in adjusting real-reactive power supply to offset power imbalance, as decisions are solely based on local measurements [16]. Without allowing for a certain amount of communication, the local dispatch decisions may not render efficient and feasible operation for the entire microgrid. Strategies that employ communication prior to a steady-state coordination event utilizes various relaxations depending on underlying system model to obtain optimal results [17]-[21]. For instance, the complex phasor based formulation of OPF problem in [21] applies a semi-definite relaxation by eliminating the rank-one constraint. If then the resulting solution does not naturally satisfy the rank-one constraint, it proves to be infeasible. The communication signals are designed in such coordination schemes based on established decentralization algorithms such as consensus or ADMM. Some coordination strategies also involve multiple hierarchies operating in different time-scales. In references [22, 23], steady-state optimization is performed at secondary level to deliver optimal source set-points over long time intervals and droop based techniques operate at the primary level to maintain system limits such as frequency, voltages, etc in short term. For the rapidly changing load dynamics of a microgrid, significant time interval between optimal source coordination events will hinder economic operation.

For islanded systems the effect of load changes can be significant, hence fast source adjustment techniques are required to neutralize perturbations. The source coordination technique in [24] achieves this in a decentralized manner utilizing a state-space model of the microgrid system. However the power sharing scheme of the aforementioned method is not guaranteed to be optimal, as non-convexities arising from nonlinear terms (e.g. sine, cosine) of state variables are not dealt with. For radial DNs, a decentralized problem formulation with transformed phasors that overcomes all but one non-convex constraint is relaxed and solved as a second-order cone program (SOCP) in [26]. However, the feasibility of the solution with respect to actual constraints is not guaranteed in this method.

1.2   Problem Statement and Thesis Objectives

The seamless operation of a microgrid requires appropriate coordination of sources during both *transient* and *steady-state* operation to maintain the power balance and system limits. Over the years, there has also been a remarkable increase in number and variety of distributed sources such as photo-voltaic devices, micro-turbines and electric vehicles capable of injecting surplus power into the DN to participate in energy trade [27]. This poses a challenge in dispatching sources with centralized commands, as this technique prove not to be scalable due to heavy computational burden and communication overheads. Centralized coordination of sources is expected to be slow and occurring over long time horizons, much like the conventional economic dispatch of large machines. On the contrary, the load-supply dynamics in a microgrid dictates that coordination of sources be performed at a much smaller time-scale to sustain feasible and efficient steady-state operation. There are also non-convexities associated with OPF formulations in microgrids that need to be effectively overcome. In light of these fundamental challenges, the objectives of the thesis are outlined as follows:

- Decomposing the microgrid OPF problem into distinct subproblems that can be solved by intelligent bus devices in a decentralized manner for local sources with minimal peer-

to-peer communication, thereby enhancing reliability and allowing expansion with seamless plug-n-play.

- Introducing a near real-time and highly granular coordination scheme for a stand-alone microgrid that directly delivers input voltage set-points in DQ frame for inverter based sources. It can be used in tandem with prevalent DQ parameter based transient control strategies to ensure sustained, stable and cost-effective operation in a microgrid with frequently varying demand-supply characteristics.

- Proposing an algorithm for feasible minimal cost power allocation of DGs in active distribution networks which is instrumental in facilitating peer-to-peer energy trading and employing low emission sources.

- Using a clear mathematical approach to leverage hidden convexities of OPF problems in different operational models of the microgrid using established theories

- Demonstrating superior feasibility and convergence of decentralized optimization algorithms with simulation based studies on practical microgrid parameters.

1.3   Thesis Outline

The rest of the chapters in this thesis discusses the detailed methodology of accomplishing the aforementioned thesis objectives and addressing the challenges present in the existing literature on source dispatch in microgrids. The sequence of the chapters and a brief description of their content are given below:

- Chapter 2 contains the mathematical approach to obtain two separate algorithms for feasible steady-state operation of an islanded microgrid which are related by the underlying state space model in DQ frame of reference used to simulate the microgrid system. The power injection from a source is defined in terms of its voltage and current injection in this model. The distinct benefits of each algorithm are discussed and comparison with recent works in the relevant literature are presented.

- Chapter 3 presents a similar mathematical approach for decentralization and convexification of a separate OPF problem where line power flow and source power injection are directly incorporated as optimization variables. This model is suitable and well-established in existing literature to simulate the operational characteristics of grid-connected microgrid systems (or active DNs).

- Chapter 4 discusses the contributions of this thesis to existing literature and future avenues of research evolving from this work.

Chapter 2

Decentralized Coordination of VSCs in Islanded Microgrid

In the broader vision of self-healing smart grids, the modular energy-independent networks with DERs in close geographical proximity to the electrical loads are called microgrids [1]. In theory, microgrids can transition between grid-connected and islanded mode, to isolate the system from upstream faults and reduce outages by meeting loads with local generation. In islanded mode, stable and efficient operation of the microgrid is vulnerable to relatively smaller changes in load or injection capabilities, which necessitates frequent reconfiguration of sources to maintain system limits and efficient power sharing [5].

This chapter covers microgrid modelling techniques and novel coordination algorithms that enable decoupling of the OPF problem. Also, results of simulation studies carried out on realistic microgrid parameters are presented to highlight performance aspects of the proposed decentralized coordination techniques.

2.1   Physical Elements and Mathematical Model

The microgrid model utilized to formulate the OPF problem and performing subsequent simulations was adopted from reference [24]. As such, the microgrid is fragmented into subsystems

with local loads and injection capabilities, connected to neighbouring buses in a serial network graph of n such subsystems.
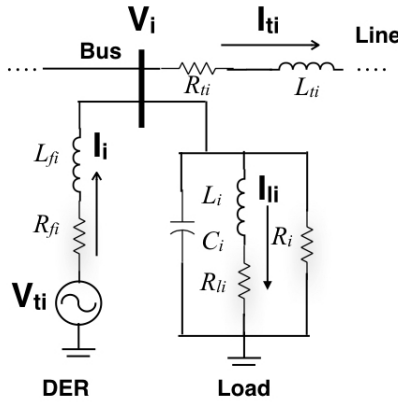
Figure 2.1: Single-line diagram of sub-system i.

Each subsystem in our microgrid model comprises of a lumped load, tie lines to neighbouring buses and a DER, represented as a controllable AC voltage source [24]. These elements are shown in Fig. 2.1. The DER in the microgrid is a combination of an energy source buffered by storage system and a voltage source converter (VSC) that lends controllability to the AC side voltage. When a sizable energy storage system (ESS) is used, DERs that inject power into the microgrid can be considered dispatchable [28]. Each DER has a voltage rating of 0.6 KV and a power rating between 1.2 to 2.5 MVA. The DER is then connected to the local bus via a series RL filter and a 0.6/13.8 kV wye-delta transformer [24]. As we use a per-unit measurement system for our study, the RL filter parameters and the transformer impedance are lumped together as resistance, R_{fi} and inductance, L_{fi}.

The constant-impedance load model is composed of three parallel branches of lumped resistances, inductance and capacitance [24, 29] . Resistive loads such as heaters, filament lamps, etc. are accounted for by the resistive component, R_i. The RL branch consisting of resistance, R_{li} and inductance, L_i represents the predominantly inductive motor loads which constitute a major share of the domestic and industrial loads [30]. Loads with rapid dynamic variation of inductance are not accounted for in this model. Lastly, the capacitance C_i is the combination of stray capacitances of lines, capacitive loads such as electrostatic precipitators and shunt capacitances for power factor correction. The tie lines connecting the subsystem to neighbouring

subsystem are modelled as a resistance, R_{ti} and an inductance, L_{ti} in series [31]. The quantities of these parameters are characteristic of the reactance-to-resistance ($\frac{X}{R}$) ratio in distribution lines with active injection [32]. A hardware-in-the-loop implementation of a microgrid of similar parameters has been presented in [25].

The state of a subsystem, i for all $i \in n$ in the microgrid at a given time is defined by the variables: $\{V_i(t), I_i(t), I_{li}(t), I_{ti}(t)\}$. Here, $V_i(t)$ is the voltage at the bus that is seen by the loads. $I_i(t)$ is the current injected into the microgrid by the DER. $I_{li}(t)$ is the current in the RL branch of the load and $I_{ti}(t)$ is the line current flowing out of the bus into subsequent subsystem, $i + 1$. The controllable input voltage of the DER is denoted by $V_{ti}(t)$. Applying Kirchoff's current and voltage laws on the microgrid model circuit in Fig. 2.1, the time domain state-space equations for the operation of the microgrid are obtained as shown below [24]:

$$\frac{dV_{i,abc}}{dt} = -\frac{V_{i,abc}}{R_i C_i} + \frac{I_{i,abc}}{C_i} - \frac{I_{Li,abc}}{C_i} - \frac{I_{ti,abc}}{C_i} + \frac{I_{ti-1,abc}}{C_i}$$

$$\frac{dI_{i,abc}}{dt} = -\frac{V_{i,abc}}{L_{f,i}} - \frac{R_{f,i}}{L_{f,i}} I_{i,abc} + \frac{V_{ti,abc}}{L_{ti}}$$

$$\frac{dI_{Li,abc}}{dt} = \frac{V_{i,abc}}{L_i} - \frac{R_{li}}{L_i} I_{Li,abc}$$

$$\frac{dI_{ti,abc}}{dt} = \frac{V_{i,abc}}{L_{ti}} - \frac{V_{i+1,abc}}{L_{ti}} - \frac{R_{ti}}{L_{ti}} I_{ti,abc} \tag{2.1}$$

where subscript abc appended to the variables denotes the three phase components of the state vectors. In addition, the variables containing the subscript $i - 1$ and $i + 1$ belong to the preceding and succeeding subsystems respectively in a serial configuration. These first order differential equations dictates the physical operational conditions of the microgrid. However, non-linearities associated with the sinusoidal state variables hinders tractable analysis of the DER set-points, V_{ti} for all $i \in n$. In order to avoid the computational burden of solving the optimization problem in its current state, we apply the following Park's transformation matrix on the state-space equations to project the state variables, K_{abc} to a synchronously rotating

direct-quadrature (DQ) frame of reference as follows [33]:

$$
K_{dq} = \frac{2}{3} \begin{pmatrix} \cos\theta & \cos\left(\theta - \frac{2}{3}\pi\right) & \cos\left(\theta + \frac{2}{3}\pi\right) \\ -\sin\theta & -\sin\left(\theta - \frac{2}{3}\pi\right) & -\sin\left(\theta + \frac{2}{3}\pi\right) \\ \frac{1}{\sqrt{2}} & \frac{1}{\sqrt{2}} & \frac{1}{\sqrt{2}} \end{pmatrix} K_{abc}
$$

The rotational position, θ of the rotating frame of reference must be consistent among the local agents solving the microgrid OPF problem for exact representation of the state variables in DQ frame. To this end, each agent is assumed to be equipped with an internal oscillator to generate a reference angle for the transformation matrix which can then be synchronized among all the agents in the microgrid to prevent drips over extended periods [34, 35]. For a microgrid of significant geographical span, this can be accomplished by exploiting a globally broadcasted signal such as GPS. Applying the aforementioned transformation, the equations characterizing the underlying voltage-current balance of the microgrid network in DQ frame of reference can be written as:

$$
\frac{dV_{i,dq}}{dt} = -\frac{V_{i,dq}}{R_i C_i} + \begin{bmatrix} 0 & w \\ -w & 0 \end{bmatrix} V_{i,dq} + \frac{I_{i,dq}}{C_i} - \frac{I_{Li,dq}}{C_i} - \frac{I_{ti,dq}}{C_i} + \frac{I_{ti-1,dq}}{C_i}
$$

$$
\frac{dI_{i,dq}}{dt} = -\frac{V_{i,dq}}{L_{fi}} - \frac{R_{fi}}{L_{fi}} I_{i,dq} + \begin{bmatrix} 0 & w \\ -w & 0 \end{bmatrix} I_{i,dq} + \frac{V_{ti,dq}}{L_{fi}}
$$

$$
\frac{dI_{Li,dq}}{dt} = \frac{V_{i,dq}}{Li} - \frac{R_{li}}{L_i} I_{Li,dq} + \begin{bmatrix} 0 & w \\ -w & 0 \end{bmatrix} I_{Li,dq}
$$

$$
\frac{dI_{ti,dq}}{dt} = \frac{V_{i,dq}}{L_{ti}} - \frac{V_{i+1,dq}}{L_{ti}} - \frac{R_{ti}}{L_{ti}} I_{ti,dq} + \begin{bmatrix} 0 & w \\ -w & 0 \end{bmatrix} I_{ti,dq} \tag{2.2}
$$

In Eq. 2.2, the state variables have subscripts dq to denote the two orthogonal components in direct and quadrature axis that results from the Park's transformation. Combining the equations above for each subsystem, we attain the state-space representation of the entire microgrid

which can be briefly expressed as:

$$\dot{z} = Az + Bu \tag{2.3}$$

where $z = [z_1 \ldots z_i \ldots z_n]^T$ is composed of state variables $z_i = [V_i, I_i, I_{Li}, I_{ti}]$ and $u = [V_{t1} \ldots V_{ti} \ldots V_{ti}]$. The state matrix, A and the input matrix, B depends on the microgrid model parameters (e.g. R_i, L_i, R_{fi}, L_{fi}, etc.). Analysis of the state matrix A reveals that the poles of the system lie in the negative half of the complex plane for the circuit parameters adopted from reference [24] which are listed for convenience in the Appendix B. This implies that the system is asymptotically stable and the state variables z settle to constant values over time [36]. This is the steady-state of the system in which $\dot{z} = 0$ and hence, the microgrid physical constraint equations in (2.2) reduce to linear convex equations that allow for tractable steady-state analysis.

2.2 Cyber-Physical Interactions

In today's era of Internet-of-Things (IoT), power entities are typically equipped with intelligent devices [37]. Our coordination scheme leverages computation and communication capabilities of these localized cyber entities that we will refer to as *bus agents* henceforth. Decentralization of the process relies on local bus agents engaging in minimal peer-to-peer communication. A simplified pictorial representation of the cyber agents and their communication scope is shown in Fig. 2.2.

During the coordination process, each bus agent acquires local parameters from the DER and loads, and exchanges few critical variables with the neighbouring agents. Typical communication delays in IEEE standardized wireless networks (e.g. ZigBee protocol) are between 8ms to 30ms for a single hop data exchange [38, 39]. However, in our model bus agents will conform to a conservative communication time interval of 100ms to exchange necessary information with neighbouring buses. State variables communicated between peers will be discussed elaborately in chapter 2.3.2. Local solutions computed are iteratively updated based on
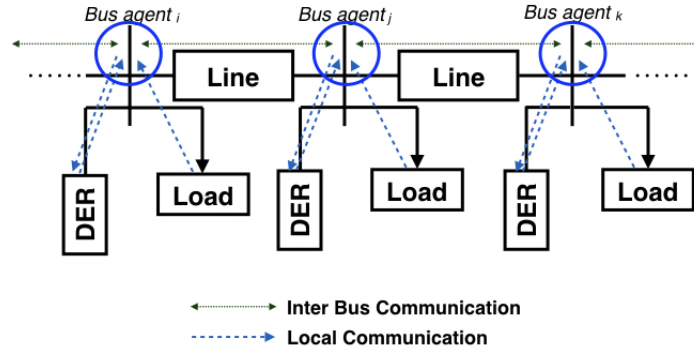
Figure 2.2: A cyber-physical microgrid.

information from peers so as to heed the operational state of the entire microgrid. Eventually the solutions converge and the agent attains the final actuation set-point for the DER voltage, V_{ti} for all $i \in n$. This coordination process is done recurrently to maintain efficient and feasible steady-state operation under impending load changes or variation in generation capabilities. Furthermore, the decentralized coordination process leveraging low latency communication schemes allows for seamless plug-and-play of modules, hence permitting unproblematic expansion of the microgrid.

2.3   Problem Formulation and Decoupling

This section first covers the general formulation of the microgrid steady-state optimization problem incorporating the voltage-current balance equations discussed in previous section and other functional constraints accounting for bus voltage regulations and DER availability. Following that, we propose a strategy to decentralize the source coordination problem for the *bus agent* in each subsystem. This requires iterative minimization and information exchanges with neighbours to eventually converge to a minimal cost, feasible solution for the entire microgrid.

2.3.1   Problem Formulation

The general purpose of any arbitrary optimization problem is to minimize a specific objective cost whilst ensuring the solution to the problem belongs to a feasible set defined by the con-

straints of the problem. For microgrids, the objective of the problem can have numerous forms including minimizing line losses, minimizing unit power cost, minimizing carbon emission from sources, etc. The problem could also have one or more of these as optimization objective [40]. In our formulation of the microgrid optimal power flow problem, the objective is a function of the local states for each subsystem, i. Hence, the overall microgrid optimization problem for this study is formulated as such :

$$P_{OC} : \underset{V,I,I_L,I_t,V_t}{\text{minimize}} \sum_{i \in n} f_i(V_i, I_i, I_{Li}, I_{ti}, V_{ti})$$

subject to: $\forall\, i \in n$

$$\frac{-V_{i,dq}}{R_i C_i} + \begin{bmatrix} 0 & w \\ -w & 0 \end{bmatrix} V_{i,dq} + \frac{I_{i,dq} - I_{Li,dq} - I_{ti,dq} + I_{ti-1,dq}}{C_i} = 0 \qquad (C1)$$

$$(1 - \mathbb{I}_{empty}(i))\left(-\frac{V_{i,dq}}{L_{f,i}} - \frac{R_{f,i}}{L_{f,i}} I_{i,dq} + \begin{bmatrix} 0 & w \\ -w & 0 \end{bmatrix} I_{i,dq} + \frac{V_{ti,dq}}{L_{fi}} \right) = 0 \qquad (C2)$$

$$\frac{V_{i,dq}}{Li} - \frac{R_{li}}{L_i} I_{Li,dq} + \begin{bmatrix} 0 & w \\ -w & 0 \end{bmatrix} I_{Li,dq} = 0 \qquad (C3)$$

$$\frac{V_{i,dq}}{L_{ti}} - \frac{V_{i+1,dq}}{L_{ti}} - \frac{R_{ti}}{L_{ti}} I_{ti,dq} + \begin{bmatrix} 0 & w \\ -w & 0 \end{bmatrix} I_{ti,dq} = 0 \qquad (C4)$$

$$I_{i,dq}\mathbb{I}_{empty}(i) = 0 \qquad (C5)$$

$$0.95^2 \leq V'_{i,dq}V_{i,dq} \leq 1.05^2 \qquad (C6)$$

In the above formulation, the constraints $(C1)$ - $(C4)$ are directly substituted from Eq. 2.2. These constraints represent the physical interdependencies of the microgrid components during steady-state operation. It can be easily observed that the given equations are not separable for a subsystem due to the dependence on neighbouring state variables, I_{ti-1} and V_{i+1}. This is the challenge presented to the decentralization of the optimization problem. Next, constraint $(C5)$ becomes active whenever the binary indicator variable, $\mathbb{I}_{empty}(i)$ takes a value of 1 indicating insufficient state-of-charge (SoC) of the associated DER battery storage. This will cause loss

of controllability of the AC side voltage of the DER. In such situations, the constraint ($C5$) forces the current injection, I_i from the respective DER to 0 and renders it unavailable for coordination. The indicator variable, $\mathbb{I}_{empty}(i)$ also takes constraint ($C2$) out of consideration when V_{ti} need not be computed, as there is no local DER. The final vital constraint of the steady-state optimization problem is for regulation of bus voltage within standard quality bounds for distribution systems, which is expressed as constraint ($C6$) [41]. The magnitude of the bus voltage phasor in *abc* frame is equal to the Euclidean norm of vector, $\|V_{dq}\|$ in DQ frame. In order to remove the associated square root from constraint ($C6$), the bounds are squared in value. For quadratically bounded regions, the basic condition for convexity of closed sets is not met. The definition of convex sets, C states that a line connecting any two points within the set must lie in the set or formally $\{\forall p_1, p_2 \in C, 0 \le \lambda \le 1 \Rightarrow \lambda p_1 + (1-\lambda)p_2 \in C\}$ [42]. The set defined by quadratic bounds such as of ($C6$) is shown in Fig. 2.3 and can be clearly seen to be defying the definition of convex sets.
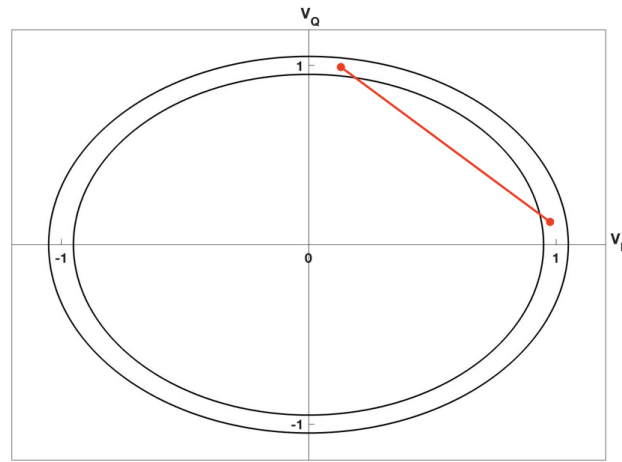
Figure 2.3: Pictorial Representation of non-convexity in ($C6$)

2.3.2   Decoupling of the Optimization Problem

The general optimization problem of a microgrid can be solved by a central entity in given form, P_{OC} using heuristic techniques or applying convex relaxations on the non-convex constraint ($C5$). However, such centralized coordination methods require communication of all essential states of the microgrid to the central agent prior to each coordination event. This may require establishing communication framework over a large area, incurring significant information exchange and computational overheads for the central agent. Thus, the problem may be rendered intractable for a fairly large microgrid. In contrast, the decentralized technique we propose can solve the optimization problem with minimal exchange of information between neighbouring nodes and splits the computational burden among participating all agents. Due to this, it is possible to solve P_{OC} frequently (i.e. timescale of seconds) to reconfigure sources depending on ongoing system changes and utilizing short span communication.

In order to formulate P_{OC} as a decentralized problem, we employ the decomposability extended by the ADMM algorithm. Application of ADMM to decompose optimization problems has already been shown in works such as [19, 21]. This requires each bus agent i to maintain two sets of variables called local and perspective variables. In our optimization problem, the local variables x_i are comprised of:

$$x_i = \{V_i^x, I_i^x, I_{Li}^x, I_{ti}^x, V_{ti}^x\} \tag{2.4}$$

where the subscript dq is eliminated from the notation for brevity. This set of variables can be used to express constraints in P_{OC} that are composed of local variables to a subsystem (e.g. constraints ($C5$), ($C6$)). Let the set $\mathcal{X}_i$ contain all feasible points defined by one or more of these local constraints. Then, the local variables x_i must belong to the feasible set $\mathcal{X}_i$.

In case of constraints ($C1$)-($C4$) in the optimization problem, they are composed of non-local states (I_{ti-1}, V_{i+1}) which prevents the separability of the problem for each individual agent. To overcome this each bus agent, i maintains another set of variables called perspective variables:

$$y_i = \{ V_{i,i}^y, V_{i+1,i}^y, I_{i,i}^y, I_{Li,i}^y, I_{ti,i}^y, I_{ti-1,i}^y, V_{ti,i}^y\} \tag{2.5}$$

where the first term of subscript denotes perspective of and the second term of subscript denotes perspective from. For example, the variable $V_{i+1,i}$ is perspective of the bus voltage of bus $i + 1$ from the agent at bus i. Through perspective variables, each agent essentially maintains a copy of its local variables and guesses of neighbouring variables that are required to completely express the non-separable constraints P_{OC}. The perspective variables y_i must belong to a feasible set, $\mathcal{Y}_i$ defined by one or more of the constraints in problem P_{OC}. Feasible set $\mathcal{Y}_i$ can incorporate any local constraints (such as $(C2), (C3), (C5), (C6)$) or non-local constraints (such as $(C1), (C4)$), unlike the feasible set $\mathcal{X}_i$ which can only be defined by local constraints.

Eventually the value of the perspective variables, y must be equal to their actual local states, x, and this is achieved by introducing the following consensus constraint to a new all-encompassing problem formulation [43]:

$$\mathcal{P}_S : \underset{x_i \in \mathcal{X}_i \,, \, y_i \in \mathcal{Y}_i}{\text{minimize}} \sum_{i \in n} f_i\,(x_i)$$

$$s.t. \ \forall \ i \in n$$

$$V_{i,i}^y = V_i^x \,, \ V_{i+1,i}^y = V_{i+1}^x \,, \ I_{i,i}^y = I_i^x \,, \ I_{Li,i}^y = I_{Li}^x \,,$$

$$I_{ti,i}^y = I_{ti}^x \,, \ I_{ti-1,i}^y = I_{t,i-1}^x \,, \ V_{ti,i}^y = V_{ti}^x$$

The ADMM optimization problem, P_S incorporates all microgrid constraints of P_C through feasible sets $\mathcal{X}_i$ and $\mathcal{Y}_i$ within which the local variables, x_i and perspective variable, y_i must lie respectively. These variables are then coupled together through the consensus constraints in P_S which will be briefly expressed as Mx=Ny now onwards. To comprehend how this ADMM formulation allows us decoupling of the problem, we must construct the augmented Lagrangian function of P_S as shown:

$$\mathcal{L}_\rho^S(x, y, v) = \sum_{i \in n} f_i(x_i) + v^T(Mx - Ny) + \frac{\rho}{2} \|Mx - Ny\|_2^2$$

$$= \sum_{i \in n} f_i(V_{ti}^x, \ V_i^x) + v_{i,i}^V (V_i^x - V_{i,i}^y) + v_{i+1,i}^V (V_{i+1}^x - V_{i+1,i}^y) + v_{i,i}^I (I_i^x - I_{i,i}^y)$$

$$(2.6)$$

$$+ \; v_{i,i}^{I_L} \, (I_{Li}^x - I_{Li,i}^y) \; + \; v_{i,i}^{I_t} \, (I_{ti}^x - I_{ti,i}^y) \; + \; v_{i-1,i}^{I_t} \, (I_{t,i-1}^x - I_{ti-1,i}^y) \; + \; v_{i,i}^{V_t} \, (V_{ti}^x - V_{ti,i}^y)$$

$$+ \; \frac{\rho}{2} \, (V_i^x - V_{i,i}^y)^2 \; + \; \frac{\rho}{2} \, (V_{i+1}^x - V_{i+1,i}^y)^2 \; + \; \frac{\rho}{2} \, (I_i^x - I_{i,i}^y)^2 \; + \; \frac{\rho}{2} \, (I_{Li}^x - I_{Li,i}^y)^2$$

$$+ \; \frac{\rho}{2} \, (I_{ti}^x - I_{ti,i}^y)^2 \; + \; \frac{\rho}{2} \, (I_{t,i-1}^x - I_{ti-1,i}^y)^2 \; + \; \frac{\rho}{2} \, (V_{ti}^x - V_{ti,i}^y)^2 \tag{2.7}$$

where v is the dual variable associated with the consensus constraint and ρ is the penalty parameter to enforce strict convexity on $\mathcal{L}_\rho^S(x, y, v)$ [43]. ρ is a user defined constant that is required to be *positive* for convergence of the problem. Each bus agent will tackle the above problem by separating it into two subproblems that solves for variables x_i and y_i successively, and updates the dual variables, v based on the difference $Mx - Ny$ in order to reach consensus (i.e. when the perspective variables have same values as their corresponding local variables). The steps in the iterative process of solving the ADMM problem, P_S are shown below:

$$x_i^{k+1} = \operatorname*{argmin}_{x_i \in \mathcal{X}_i} \mathcal{L}_p^S(x, y^k, v^k) \tag{U1}$$

$$y_i^{k+1} = \operatorname*{argmin}_{y_i \in \mathcal{Y}_i} \mathcal{L}_p^S(x^{k+1}, y, v^k) \tag{U2}$$

$$v_i^{k+1} = v_i^k + \rho(Mx^{k+1} - Ny^{k+1}) \tag{U3}$$

In the above equations, the local variable update, x^{k+1} is the minimization of the Lagrangian function to find a solution within feasible set, $\mathcal{X}_i$. Prior to the update only the necessary variables of $k - th$ iteration needed from neighbouring subsystems, $\{I_{ti,i+1}^y, v_{i,i+1}^I, V_{i,i-1}^y, v_{i,i-1}^V\}$ are communicated to the agent. Similarly for the perspective variable update , y^{k+1} some variables in x^{k+1} of the current iteration, $\{I_{ti-1}^x, V_{i+1}^x\}$ need to be communicated to the bus agent from neighbouring subsystems. Both these minimization sub-problems are solved for variables that are locally maintained at a particular bus agent, hence this is now a completely decentralized problem. The third step is the update of the dual variable associated with the consensus constraint, $Mx - Ny$.

Repeating this process the bus agents refine their local and perspective variables until the residual $\|Mx - Ny\|_2$ of the consensus constraint fall below a pre-defined threshold value, ϵ. At

this point convergence is achieved, which implies that the terms $v(Mx - Ny)$ and $\rho\|Mx - Ny\|_2^2$ tend to 0 causing the Lagrangian objective function $\mathcal{L}_\rho^S$ to reduce to the objective in P_{OC}. For a convex problem reformulation of P_{OC} (covered in Chapter 2.4 and 2.5), it has been shown that the ADMM iterations will always converge to a feasible solution for a strictly positive ρ value, which is a user-defined constant parameter maintained by all bus agents in the microgrid. The convergence rate has been demonstrated to be linear with respect to number of *bus agents*, n in the system (i.e. $O(n)$) in reference [19] and verified through our simulations. Thus, employing ADMM decomposition on the optimization problem allows us to compute optimal states, x_i' locally through iterative refinement of the local estimates using communication.

The decentralized problem formulation is designed such that even when a node is lost for communication in the serial network system due to some failure, the coordination process can still continue in separate blocks. This implies the subsystem associated with the failed *bus agent* will be taken off-duty by breaking its connection to the microgrid at the bus. This results in two separate, connected blocks which continues the coordination process acting as independent systems.

2.4   Decentralized Optimization via Strategic Linearization

The process of solving the microgrid steady-state optimization problem is not a straightforward one, due to non-convexity of problem, P_{OC}. In this section, we discuss approximations and linear relaxations employed to obtain a rapidly converging and convex reformulation of the problem. Simulation results obtained through application of the decentralized optimization technique are presented later in the section to assess its key performance features.

2.4.1   Linear Relaxation of Non-Convex Constraints

The convergence of the ADMM problem is contingent on the convexity of the objective function and constraints of the original optimization problem, P_{OC}, because they are subjectively incorporated in subproblems ($U1$) and ($U2$). The power supplied by a DER in the microgrid is

chosen to be proportional to the square of current injected into the bus. Assuming a linear cost function for power supplied by the DER, $K_i P_i$ the objective of the problem is formulated as:

$$f_i(x_i) = K_i [I_{i,d}^2 + I_{i,q}^2] \tag{2.8}$$

In Eq. 2.8, $I_{i,d}$ and $I_{i,q}$ are the *dq* components of the current injected by DER *i*, and K_i is the unit cost of the real power supplied by the respective DER. Environmental conditions of DERs (such as solar irradiance, wind speeds) may affect SoC of the battery and the cost factor, K_i associated with a DER. It can be easily determined that the hessian matrix of the objective function, $f(I_{id}, I_{iq})$ is positive-semi definite, which implies that the objective is convex. The objective function is then incorporated in the minimization subproblem (*U*1) because it depends on current injection from source, I_i which is a local variable for subsystem *i*.

Decomposition of the original microgrid optimization problem using ADMM results in two subproblems (*U*1) and (*U*2) which were introduced in chapter 2.3.2. Microgrids operational constraints (*C*1)-(*C*6) can be disseminated among these subproblems depending on the necessity of the *x* or *y* variables in forming the constraint equations. We design the ADMM optimization problem, P_S such that, the solution x^{k+1} from the x-minimization step belongs to the set defined by the bus voltage regulation constraint shown below:

$$0.95^2 \leq V_{i,D}^{x\,2} + V_{i,Q}^{x\,2} \leq 1.05^2 \tag{2.9}$$

This constraint does not satisfy the formal definition of convex sets, which has already been shown in Ch. 2.3.1 . The space between the solid black lines in Fig. 2.3 illustrates the feasible region of this equation. Hence, we propose a linear relaxation of this constraint utilizing intersecting hyperplanes to form a polytope that closely approximates the non-convex set, similar to reference [44]. We focus our analysis on a single quadrant because the total phase angle deviation between bus voltages in a typical distribution network is not more than a few degrees [45] and the frame of reference of the system can be aligned so that the V_{dq} points lie in a single quadrant. The mathematical representation of the affine constraints that replaces the

non-convex constraint ($C6$) is shown below:

$$V_{i,d}^x + V_{i,q}^x \geq 0.95$$

$$V_{i,d}^x \leq f'(\alpha_k)\left(V_{i,q}^x - \alpha_k\right) + f(\alpha_k) \ \forall \ k = 1 \ldots m \ (C6')$$

where $\alpha_k = -1.05 + \frac{2.10k}{m+1}$ and $f(\alpha_k) = \sqrt{1.05^2 - \alpha_k{}^2}$. The linear reformulation, ($C6'$) approximates the lower bound using a triangular inequality. The second equation in ($C6'$) represents an overlapping internal region of concentrated straight lines that are tangential to the outer boundary of the quadratic constraint. It can be apprehended from the pictorial representation of ($C6$) and ($C6'$) in Fig. 2.4 that, the relaxation of the lower limit of quadratic bound is not tight due a larger gap between the linear relaxation and the quadratic curve when compared to the upper limit. This leads to the risk of obtaining solutions that reside outside the original bounds. To compensate for this, we add a $-V_q$ term to the objective of the subproblem that drives the bus voltages towards the upper bound in order to avoid infeasible solutions. It has been illustrated through simulation studies presented in Ch. 2.4.2 that this algorithm is capable of retrieving solutions within the feasible bus voltage bounds when a fair lagging power factor is maintained at each bus. This essentially means that shunt capacitances should be introduced locally to somewhat counteract the voltage dipping effect of excessively increasing inductive loads. All other constraints in P_{OC} are incorporated as constraints of y-minimization
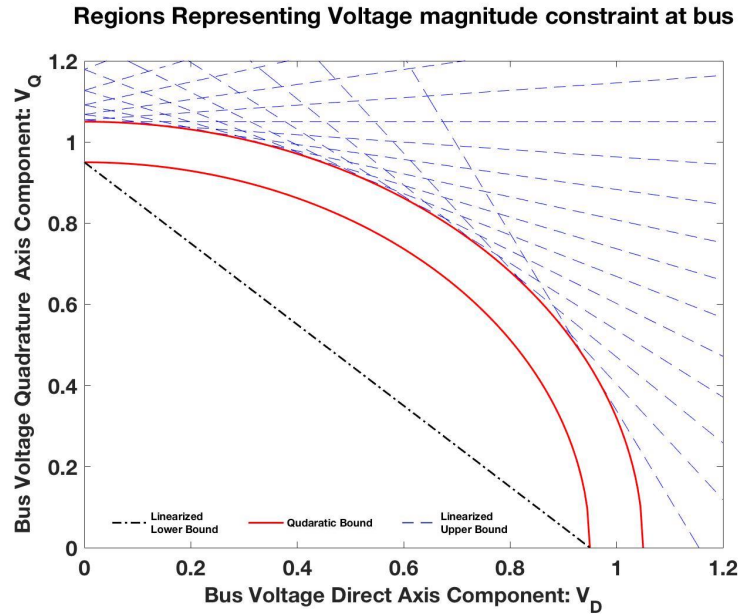
Figure 2.4: Linear relaxations for quadratic constraints.

subproblem defining the feasible set $\mathcal{Y}_i$:

$$\frac{-V^y_{i,dq}}{R_i C_i} + \begin{bmatrix} 0 & w \\ -w & 0 \end{bmatrix} V^y_{i,dq} + \frac{I^y_{i,dq} - I^y_{Li,dq} - I^y_{ti,dq} + I^y_{ti-1,dq}}{C_i} = 0$$

$$\frac{-V^y_{i,dq}}{L_{f,i}} - \frac{R_{fi}}{L_{fi}} I^y_{i,dq} + \begin{bmatrix} 0 & w \\ -w & 0 \end{bmatrix} I^y_{i,dq} + \frac{V^y_{ti,dq}}{L_{fi}} = 0$$

$$\frac{V^y_{i,dq}}{Li} - \frac{R_{li}}{L_i} I^y_{Li,dq} + \begin{bmatrix} 0 & w \\ -w & 0 \end{bmatrix} I^y_{Li,dq} = 0$$

$$\frac{V^y_{i,dq}}{L_{ti}} - \frac{V^y_{i+1,dq}}{L_{ti}} - \frac{R_{ti}}{L_{ti}} I^y_{ti,dq} + \begin{bmatrix} 0 & w \\ -w & 0 \end{bmatrix} I^y_{ti,dq} = 0$$

$$I^y_{i,dq} \mathbb{I}_{empty}(i) = 0$$

These are equivalent to the constraints $(C1)$-$(C5)$ in original problem, P_{OC} but expressed in terms of the perspective variables, y_i in this case. The constraints $(C1)$-$(C4)$ account for the microgrid steady-state operational conditions and the constraint $(C5)$ controls the unavailability of a DER for coordination.

Given the linear, convex reformulation of the problem P_{OC} , the proposed algorithm converges to a final solution satisfying the consensus constraints after $\mathcal{I}$ iterations, depending on the total number of subsystems in microgrid n. Quadratic Program (QP) with linear constraints can be very efficiently solved and demands significantly lower computational capacity compared to the more general class optimization problems (e.g. SOCP, SDP, etc.). This is the principal trade-off of employing relaxations that may yield infeasible solutions in some cases. However, primal feasibility has been observed to hold for practical load compositions rendering this technique very effective for microgrid coordination.

2.4.2   Results - Coordination Scheme I

In order to determine the performance attributes of the proposed decentralized coordination strategy, we ran various simulations in MATLAB utilizing microgrid system parameters from

reference [3]. The studies were conducted on microgrid sizes ranging from 3 to 10 subsystems to deduce convergence and feasibility aspects of the acquired solution.

Steady-State Characteristics

First we conduct time-domain studies of the model microgrid system in [3] by actuating the DERs with set-points, V_{ti} for all $i \in n$, obtained from applying the proposed algorithm. The mathematical model of the system was programmed into an ODE45 solver that yields the response of state variables with time for a step energization to voltage, V_t. The bus voltage of a respective subsystem, V_i is measured after the system is actuated with the corresponding DER input voltage, V_{ti} in the system model, Fig. 2.5 to observe the time-domain response in the microgrid.
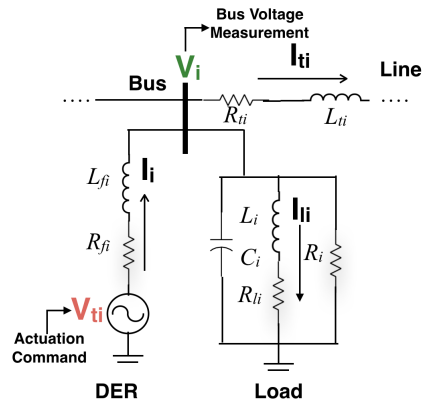
Figure 2.5: System model for result in Fig. 2.6

The bus voltages of the microgrid system shown in Fig. 2.6 (a) are observed to encounter transient oscillations before settling to constant DQ values in steady state. The constant steady-state values corresponds to the state variables obtained as solution x' of the optimization algorithm, which is expected because the mathematical form of the steady-state were incorporated as constraints in problem P_S. To confirm that these values are consistent with their actual sinusoidal form in abc phases, we also stimulate a PSCAD model of the microgrid study system with the corresponding three phase input voltage, $V_{ti,abc}$. The evolution of the bus voltages in the abc frame as shown in Fig. 2.6 (b) are of similar time scales to the DQ values and the magnitude of the sinusoids in steady state is equal to the Euclidean norm of the DQ vector. To

highlight the exactness of the frame of reference conversion in implementation, we have added data tips at $t = 0.2257s$ in both graphs of Fig. 2.6 to display the steady-state values within a coordination horizon. It is clear that the magnitude of the state variable in the *dq* frame $\sqrt{0.7030^2 + 0.7013^2} = 0.9929$ is very close to the amplitude 0.9938 of the variable in the abc frame. The differences in the values are insignificant and can be ascribed to rounding errors or differences in modelling of dynamical systems in the two separate platforms (i.e. MATLAB and PSCAD).

The substantial overshoot encountered by the system during energization of source from zero state can cause damage to the components of microgrid. To mitigate this effect, we suggest ramping up the voltage to V_t over a certain period of time [46]. Modular multi-level converters with the capability of operating over a wide range of voltages can be used for this purpose [48]. Simulations performed on the study system reveal that the overshoot of bus voltage is restrained to less than 5% of nominal value when we steadily ramp up the input voltage over a period of 1.5 cycle (where 1 cycle = 1/60 seconds for a 60 Hz system). Any further increase in the ramping period had insignificant effect in reducing the overshoot. This overshoot trend has been illustrated in Fig. 2.7
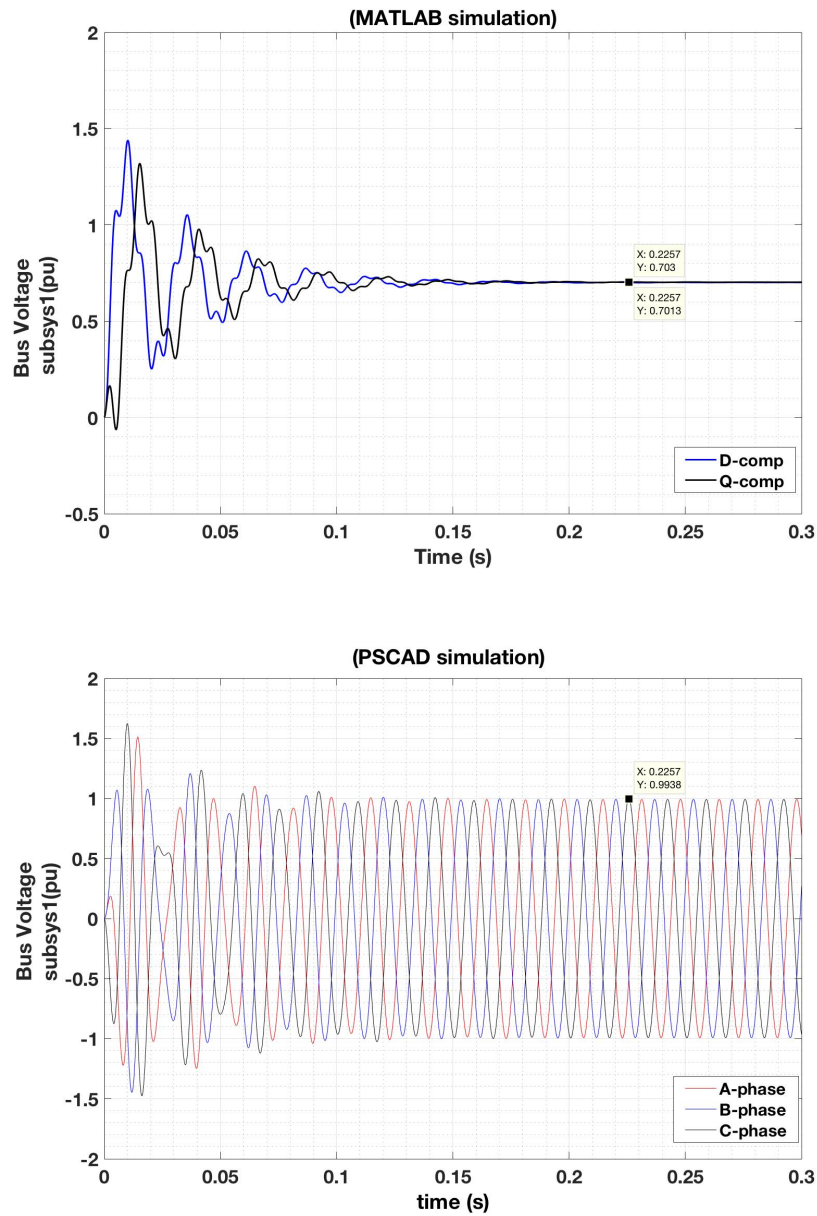
Figure 2.6: (a) Time domain response in *dq* frame (b) Time domain response in *abc* frame
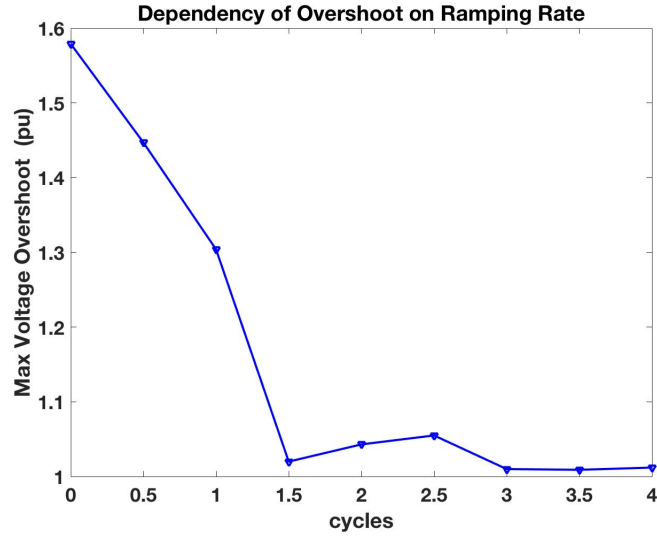
Figure 2.7: Overshoot during excitation

Convergence Study

Next we observed the effect of the size of the study system on the convergence speed of the program. Besides the three-bus microgrid system adopted from [3], we apply the decentralized coordination algorithm on a ten-bus microgrid system. The larger system is formed by arbitrarily replicating the three distinct bus types listed in Appendix A and joining them serially. Although we design and implement the coordination algorithms in this chapter for a serial network configuration, the technique for convexifying and decentralizing the problem is extendable to radial systems, which is more common in DNs. Extending the problem formulation for a radial microgrid configuration does not introduce further non-convexities as it only introduces more linear terms in the convex constraints $(C1) - (C4)$. Both the systems exhibit similar convergence pattern and attain convergence within 10 and 20 iterations respectively. This is similar to the theoretical result that convergence rate changes linearly with respect to the size of the system (i.e. $\mathbb{O}(n)$) for ADMM applied to a convex problem[19]. This superior convergence speed is crucial in realizing a highly granular coordination scheme for microgrids with frequently changing load or generation characteristics.
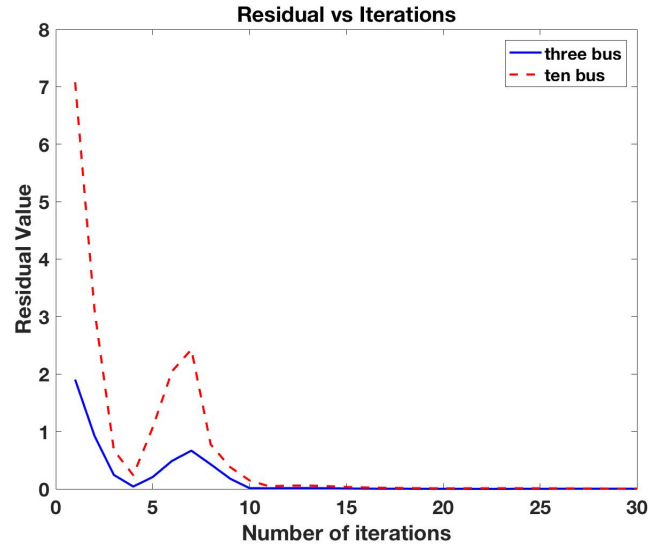
Figure 2.8: Residual vs Iteration

Feasibility Study

In our last set of simulations with this coordination scheme, we perform feasibility checks on the obtained solution for a wide range of loads on a microgrid with ten subsystems. Our solution can potentially violate standard voltage bounds mainly due to loose relaxations adopted in the inner portion of the quadratically bound region, as discussed in chapter 2.4. Inductive loads are the most influential in depressing the voltage at the bus it is drawing power from. Hence, we tested the feasibility of the solution obtained for various scenarios of increasing the inductive loading at a bus by appropriately changing the RL branch parameters of the load model. The loading was varied between 1.0 p.u. to 2.0 p.u. From observing the maximum and minimum bus voltages of the proposed solution in Fig. 2.9 (a) , it can be inferred that one or more bus voltages in the microgrid violates the voltage feasibility bounds for any increase in inductive loading over 10%.

To overcome this undesirable effect, shunt capacitances were locally added to compensate for the increased reactive power demand. It is indeed a common practice for industrial consumers with highly inductive loads to provide local compensation to avoid penalties from electrical utilities for poor load power factor at point of coupling (i.e. bus). It was observed from our simulation studies that adding shunt capacitances in the following ratios: 10% for 20%,
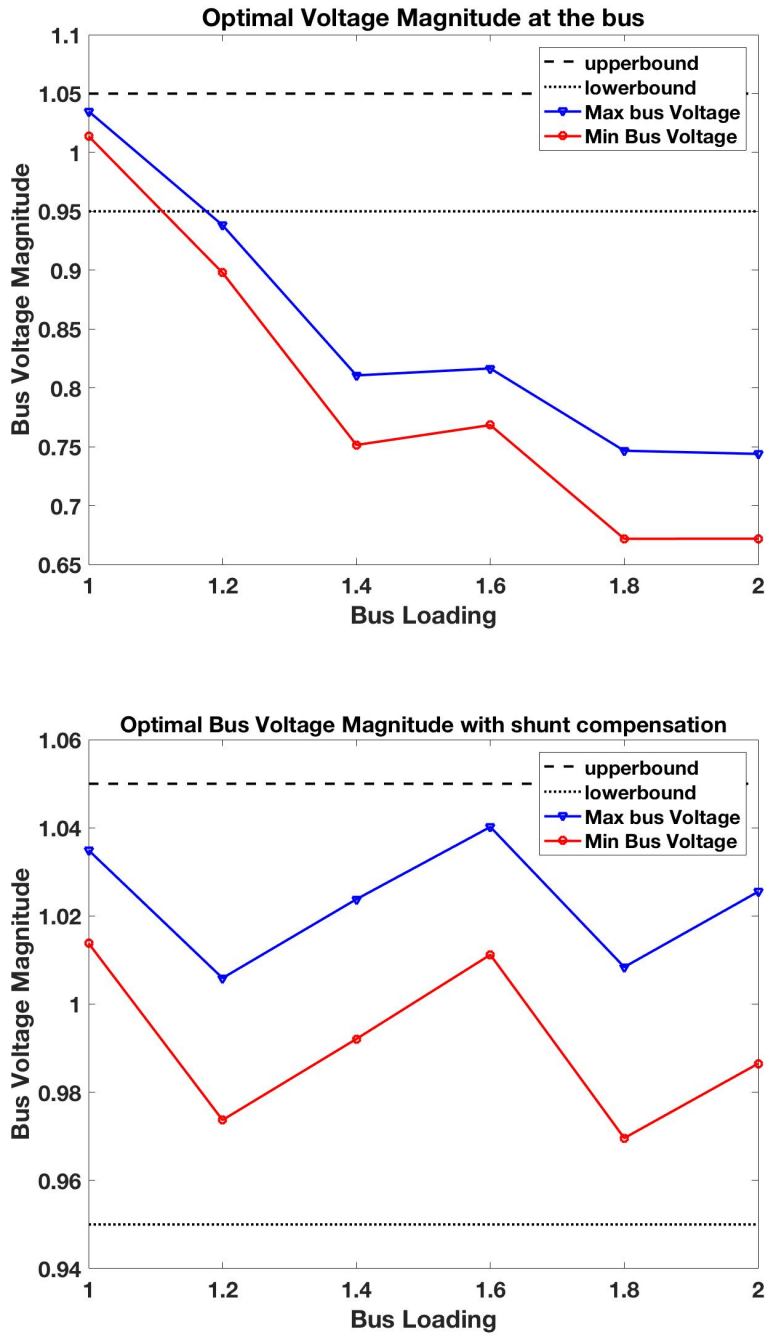
Figure 2.9: (a) Bus Voltages without capacitive shunt compensation (b) Bus Voltages with capacitive shunt compensation

30% for 40%, 50% for 60%, 60% for 80%, 70% for 80% respectively return the computed optimal solution within feasible bounds, as shown in Fig. 2.9 (b). Shunt capacitance switching is not an effective solution for motor loads that may require 3-5 times its rated reactive power during starting. However, in the coordination scheme we propose next, we overcome this by procuring dynamic reactive power support from smart inverters interfacing DERs. When the solution obtained from the relaxed convex problem is feasible with respect to the quadratic voltage constraint, it is also a solution of the original microgrid optimization problem, P_{OC}.

2.5 Decentralized Optimization via S-Procedure

In this section, we set forth an alternate formulation of the ADMM microgrid optimization problem with a convex relaxation that imposes tight restriction on the feasibility of the solution. The previous scheme is not reliable for systems which undergoes frequent and significant variations of inductive loads between coordination intervals. The repeated need for capacitor switching can be cumbersome and lead to voltage fluctuations. On the contrary, this scheme harnesses the capability of DER inverters to rapidly adjust the local reactive power support in a subsystem [47]. The results from employing this algorithm on the same microgrid model are presented to highlight improvements from the previous method and other comparable techniques in the literature.

2.5.1 Convex Relaxation and Strong Duality

First, we withdraw the approximation in constructing the objective function in the previous scheme and state the exact expression of power supplied in terms of input voltage, V_{ti} and bus voltage, V_i. The power supplied by a DER in terms of its voltage and current in a rotating dq frame is [49]:

$$P_i = \frac{3}{2} V'_{ti,dq} I_{i,dq} \tag{2.10}$$

Then, rearranging the constraint equation (C2) in P_{OC}, we can express $I_{i,dq}$ in terms of the DER input voltage, $V_{ti,dq}$ and the corresponding bus voltage, $V_{i,dq}$:

$$I_{i,dq} = \begin{bmatrix} R_{fi} & -wL_{fi} \\ wL_{fi} & R_{fi} \end{bmatrix}^{-1} \begin{bmatrix} V_{ti,dq} - V_{i,dq} \end{bmatrix} \tag{2.11}$$

Substituting the above expression in the formula for power delivered in Eq. 2.10 and assuming a linear cost function $K_i P_i$, where K_i is the normalized cost factor assigned to DER in subsystem i [50]. The generation cost function $f_i(V_{i,dq}, V_{ti,dq})$ for the source in subsystem i can

be written as:

$$f_i(V_{i,dq}, V_{ti,dq}) = \frac{\frac{3}{2}K_i}{R_{fi}^2 + \omega^2 L_{fi}^2} \begin{bmatrix} V_{i,dq} \\ V_{ti,dq} \end{bmatrix}' M_i \begin{bmatrix} V_{i,dq} \\ V_{ti,dq} \end{bmatrix} \tag{2.12}$$

$$\text{where } M_i = \begin{bmatrix} 0 & 0 & -\frac{R_{fi}}{2} & \frac{\omega L_{fi}}{2} \\ 0 & 0 & -\frac{\omega L_{fi}}{2} & -\frac{R_{fi}}{2} \\ -\frac{R_{fi}}{2} & -\frac{\omega L_{fi}}{2} & R_{fi} & 0 \\ \frac{\omega L_{fi}}{2} & -\frac{R_{fi}}{2} & 0 & R_{fi} \end{bmatrix}$$

In a convex problem, the Hessian of the doubly-differential objective function in Eq. 2.10 has to be positive semi-definite (PSD) [51]. The matrix M_i contains the respective DER filter paramters R_{fi} and L_{fi}. For a typical DER filter quality factor, the Hessian matrix M_i may have one or more negative eigenvalues. This implies that the Hessian of the objective in the microgrid cost minimization problem is not generally PSD and hence, non-convex.

Similar to the previous scheme of decomposing and decentralizing the microgrid optimization problem by applying ADMM, we separate the objective and constraint of the original problem among the x-minimization and y-minimization subproblems (U1) and (U2) introduced in chapter 2.3.2. The constraints of the equation are separated depending on the applicability of the local or perspective variables maintained in the respective subproblems and to isolate the non-convex voltage regulation constraint. First, it is important to observe that the quadratic bus voltage inequality shown in (C6) is only non-convex in the lower bound and not in the upper bound. This can be proven by first evaluating the Hessian of the inequality function in its standard form, i.e. $f_i(x) \leq 0$. The Hessian of the upper bound function $V_{id}^2 + V_{iq}^2 - 1.05^2 <= 0$ and the lower bound function $-V_{id}^2 - V_{iq}^2 + 0.95^2 <= 0$ in their standard forms are:

$$\text{Upper Bound} = \begin{bmatrix} 2 & 2 \\ 2 & 2 \end{bmatrix} \qquad \text{Lower Bound} = \begin{bmatrix} -2 & -2 \\ -2 & -2 \end{bmatrix}$$

It is clear that the second Hessian matrix corresponding to the lower bound of the quadratic inequality constraint is not positive-semi definite and therefore, it forms a non-convex set. This constraint and the non-convex objective function, $f_i(V_{i,dq}, V_{ti,dq})$ is absorbed in the subproblem $(U1)$ minimizing for x_i as these are functions of local variables of a subsystem in the microgrid. Along with the other terms in augmented Lagrangian of the optimization problem in Eq. 2.7, the subproblem $(U1)$ takes the general form of:

$$\mathcal{P}^i_{U1} : \underset{x_i \in X_i}{\text{minimize}} \; \frac{1}{2} \, x_i^T \left(A_0^i + B_0^i\right) x_i \; + \; C_0^i \, x_i$$

$$s.t. \; \underline{D_1^i} \leq \frac{1}{2} x_i^T A_1^i x_i$$

where A_0^i is the coefficient $\frac{\frac{3}{2} K_i}{R_{fi}^2 + \omega^2 L_{fi}^2} M_i$ from the cost function $f_i(V_{ti}, V_i)$. B_0^i is a diagonal matrix containing the coefficients of quadratic terms in $\mathcal{L}_\rho^S$ pertaining to x_i. The general structure of B_0^i is $2diag(2\rho, 2\rho, \rho, \rho, \rho, \rho, 2\rho, 2\rho, \rho, \rho)$ for all subsystems except for subsystems located at the ends of the physical microgrid network. For a subsystem having no neighbour $i + 1$, the 7th and 8th elements in B_0^i are set to 2ρ. Similarly for a subsystem having no neighbour $i - 1$, the 1st and 2nd elements are equal to 2ρ. C_0^i is the matrix containing the coefficients of the linear terms in $\mathcal{L}_\rho^S$ pertaining to x_i. The constraint reflects the lower bus voltage limits and is expressed in standard quadratic form where $A_1^i = 2diag(1, 1, 0, \ldots, 0)$ so that $\frac{1}{2} x_i^T A_1^i x_i = V_i' V_i$ and $\underline{D_1^i}$ represents the lower limit of the normalized bus voltage magnitude squared.

It is crucial to tackle various non-convexities in the subproblem $\mathcal{P}^i_{U1}$, so that we can obtain a converging solution to the decentralized optimization problem. The Hessian of the objective in $\mathcal{P}^i_{U1}$ is the sum of two matrices $(A_0^i + B_0^i)$. It has been mentioned earlier in this section that A_0^i is non-convex for typical DER parameters. Matrix B_0^i consists of a user defined parameter, ρ that is inherent to the augmented Lagrangian, $\mathcal{L}_\rho^S(x, y, v)$. The objective of the problem is convex, only when ρ is selected such that the Hessian is positive semi-definite (i.e. $A_0^i + B_0^i \geq 0$).

Theorem 2.5.1 *When ρ satisfies the following inequality, the objective function of $\mathcal{P}_{U1}$ is convex:*

$$\rho \geq \max_{i \in n} \left\{ \sqrt{\frac{1}{2}\left(\frac{R_{fi}K_i}{D_i}\right)^2 + \frac{1}{4}\left(\frac{wL_{fi}K_i}{D_i}\right)^2} - \frac{1}{2}\left(\frac{R_{fi}K_i}{D_i}\right) \right\} \tag{2.13}$$

Proof A matrix is said to be positive semi-definite when all the eigenvalues of the matrix are non-negative [42]. e is the eigenvalue of matrix $(A_0^i + B_0^i)$ if $det(A_0^i + B_0^i - \mathbf{I}e) = 0$ where $\mathbf{I}$ is an identity matrix. From this equation we obtain an expression of e in terms of ρ and other parameters of matrix $(A_0^i + B_0^i)$. Then, equating for ρ such that $e \geq 0$ we can derive the equation listed above. A detailed proof is listed in Appendix A of this paper.

Thus, we select ρ according to Theorem 2.5.1 to enforce convexity of subproblem $\mathcal{P}_{U1}$. As the ADMM program has been proven to converge to a solution for any non-negative ρ in reference [43], this does not contradict the fundamental purpose of the ρ parameter.

The subproblem P_{U1} is not convex despite the convexity of the objective, because it also contains the lower bound voltage magnitude constraint. The constraint has already been proven to be non-convex earlier in the section. To tackle this, we construct the Lagrangian dual function $g(\lambda)$ of problem P_{U1} where λ is the lagrangian multiplier associated with the voltage lower bound constraint:

$$g(\lambda) \; : \; \underset{x}{\text{minimize}} \; \frac{1}{2} x^T (A_0 + B_0) x + C_0 x + \lambda \left(\underline{D_1} - \frac{1}{2} x^T A_1 x \right)$$

Closed-form expression can be obtained for $g(\lambda)$ by evoking the first-order optimality condition (i.e. $\frac{\partial \mathcal{L}_{U1}}{\partial x} = 0$) where $\mathcal{L}_{U1}$ is the Lagrangian function associated with $\mathcal{P}_{U1}$. x can be expressed in terms of λ via the relation $\frac{\partial \mathcal{L}_{U1}}{\partial x} = 0$:

$$\frac{\partial \mathcal{L}_{U1}}{\partial x} = (A_0 + B_0)x + C_0 - \lambda(A_1 x) = 0; \tag{2.14}$$

$$x = -(A_0 + B_0 - \lambda A_1)^{-1} C_0 \tag{2.15}$$

where x is in terms of λ. Substituting x into $g(\lambda)$ results in the dual problem $\mathcal{D}_{U1}$:

$$\mathcal{D}_{U1}: \max_{\lambda_{U1}} \ \lambda\underline{D_1} - \frac{3}{2} C_0^T (A_0 + B_0 - \lambda A_1)^{-1} C_0$$

$$\text{s.t.} \quad \lambda \geq 0 \tag{D1$'$}$$

$$A_0 + B_0 - \lambda A_1 \geq 0 \tag{D2$'$}$$

In the dual problem, constraint $(D1')$ is a fundamental inequality relation associated with any Lagrangian multiplier, λ. The constraint $(D2')$ is a positive semi-definite relation necessary to avoid the trivial solution of $-\infty$. Given the structure of the problem, we can apply Schur's complement identity to convert the given dual problem $\mathcal{D}_{U1}$ to a semi-definite program (SDP) [42, 52]:

$$\mathcal{S}_{U1}: \underset{\lambda,\gamma}{\text{maximize}} \quad \gamma$$

$$\text{s.t.} \ \lambda \geq 0$$

$$\begin{bmatrix} A_0 + B_0 - \lambda A_1 & C_0 \\ C_0^T & \lambda\underline{D_1} - \gamma \end{bmatrix} \geq 0$$

Solving the dual problem above, we obtain the optimal dual solution which is λ^*. When we substitute this back into the closed form expression in Eq. 3.9, we get the corresponding primal solution x'. Strong duality is the phenomenon that occurs when the dual optimal value, g^* obtained solving the dual function is exactly equal to the primal optimal value, p^*. This is in most cases true only for a convex problem. However, our subproblem P_{U1} falls in the class of a special non-convex problem for which strong duality holds due to hidden convexity as described in Theorem 2.

Theorem 2.5.2 *Strong duality holds between P_{U1} and g when the primal problem P_{U1} is strictly feasible.*

Proof For a quadratically constrained quadratic program (QCQP), the theory of S-procedure

states that if there exists a $\lambda \geq 0$ such that:

$$
\begin{bmatrix} A_0 + B_0 & C_0 \\ & \\ C_0^T & -\gamma \end{bmatrix} + \lambda \begin{bmatrix} -A_1 & 0 \\ & \\ 0 & D_1 \end{bmatrix} \geq 0
$$

then, the optimal value of the dual and primal are equal ($P_{U1}^* = g^*$) regardless of the convexity of quadratic constraint. The above relationship holds when the first matrix term in the above condition is positive semi-definite (PSD). That term originates from the objective of problem P_{U1} and it is PSD when ρ is selected according to Theorem. 2.5.1

Finally, it is acknowledged that the subproblem ($U2$) only contains the linear convex constraints ($C1$)-($C5$) and the convex quadratic upper bound inequality of constraint ($C6$) in P_{OC}. The objective of the subproblem has non-mixed quadratic terms which only contains $\rho > 0$ as coefficients. This results in a diagonal Hessian matrix with only positive elements, thus implying the objective is convex.

Alg 1: Decentralized Microgrid Coordination for Bus Agent i

Initialize: $x_i \leftarrow 0$, $y_i \leftarrow 0$, $v_i \leftarrow 0$, $k \leftarrow 0$, $r_i^{k+1} \leftarrow \infty$, $\rho \in Eq.$ 2.13, $\mathcal{N}_i \leftarrow$ Neighbours of i
while $r_i^{k+1} > \epsilon$ **do**
    $x_i^{k+1} \leftarrow \underset{x_i \in \mathcal{X}_i}{\text{argmin}} \, \mathcal{L}_\rho^i(x_i, y^k, v_n^k)$
    Solve for λ^* from S_{U1}; Set $x_i^{k+1} = (A_0 + B_0 - \lambda^* A_1)^{-1} C_0$
    - Broadcast to all $\mathcal{N}_i$ the computed x_i^{k+1}
    $y_i^{k+1} \leftarrow \underset{y_i \in \mathcal{Y}_i}{\text{argmin}} \, \mathcal{L}_\rho^i(x_n^{k+1}, y, v_n^k)$
    - Broadcast to all $\mathcal{N}_i$ computed y_i^{k+1}
    $v_i^{k+1} \leftarrow v_i^k + \rho(x_i^{k+1} - y_i^{k+1})$
    - Broadcast to all $\mathcal{N}_i$ computed v_i^{k+1}
    - Compute residuals: $r_i^{k+1} \leftarrow \|M_i x_i^{k+1} - N_i y_i^{k+1}\|$
    - $k \leftarrow k + 1$
end while

Applying the convex relaxations introduced above to this problem, we iterate through the ADMM steps ($U1$) − ($U3$) to recurrently minimize for variables x^k and y^k as shown in Alg. 1. The solutions eventually converge (as discussed in Ch. 2.3.2), thereby delivering the solution

x^* to the original microgrid problem, P_{OC} in a decentralized manner which is guaranteed to be feasible due to the exact relaxation.

2.5.2 Results: Coordination Scheme II

Various studies conducted by applying the proposed coordination scheme on our microgrid study system will be presented in this section to establish its performance features. The convergence and feasibility studies are ran across larger system size than the previous case (upto 30 buses as shown in Fig. 2.10). The bigger microgrids are formed by an arbitrary replication and combination of the 3-bus types which is detailed in Appendix B. It is important to note that results pertaining to time-domain characteristics in the microgrid (shown in chapter 2.4) holds same for set-points calculated by any scheme. Hence, they are not separately presented in this section.

Figure 2.10: 30-bus line diagram
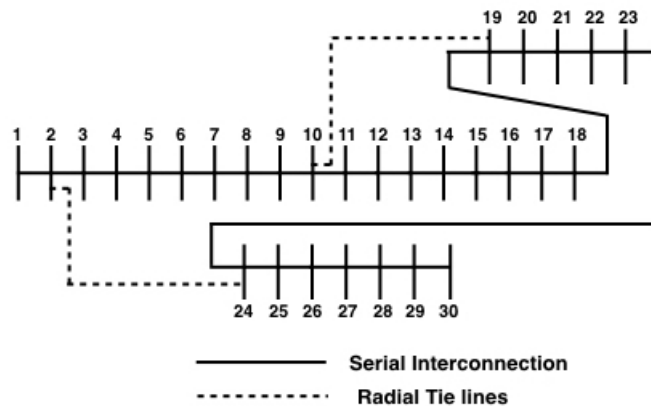
Convergence Study

The convergence rate of the proposed decentralized algorithm directly affects how frequently the sources can be coordinated in the microgrid. To determine quantitative results for convergence, we applied the decentralized coordination algorithm on microgrids with 3, 10, 20 and 30 subsystems. The results in Fig. 2.11 shows the descend of residual with the number of

ADMM iterations. For each microgrid system, our program tracks the number of iterations it takes for the residual value shown in Alg. 1 to fall below the threshold, ϵ. Each iteration in the iterative ADMM algorithm consists of three steps, $(U1)$-$(U3)$. Between each step a coordinating agent needs to communicate with neighbouring nodes which are generally one hop away. Typical communication delay associated with this information exchange is usually between 8 to 30ms. The first two steps in an iteration are solving subproblems, P_{U1} and P_{U2} over x and y respectively. These problems belong to the Semi-Definite Program (SDP) and Quadratic Program (QP) optimization classes and solving these entail a computational cost of $O(b^3)$ through interior point methods. The third step is a linear combination $O(b)$ to update the dual variable, ν for the subsequent step. Given that b ranges from 5 to 10 variables for a given subsystem, these subproblems can be solved in a fraction of millisecond given the computational power embedded in decentralized intelligent devices. We consider a conservative time delay of $100ms$ for each step in one iteration of the coordination process to account for worst case computational and communication delays. This means each iteration is performed over $0.1 * 3 = 0.3$ seconds For the 30-bus microgrid system, we observed that the solutions reach sufficient convergence by 160 iterations. This implies that the time required for the optimization program to deliver new set-points is 48 seconds. The time elapsed between two coordination events for the given 30-bus microgrid should therefore, be larger than the convergence time calculated.

Next we present the outcome of defining different values of ρ on the convergence of system. For the given study, we fix our microgrid system to five buses. The selected ρ, which is a quadratic coefficient in $(U1), (U2)$ and a dual variable step size in $(U3)$, affect the rate of convergence and can be tuned for improving convergence speed. In general, a large ρ tends to result in small primal residuals due to imposing large penalty for violation of primal feasibility. However, a high ρ value also tends to cause large variations in the dual variable which manifests through larger initial overshoot of residual, as shown in Fig. 2.12. There is a strict positive lower bound for ρ to enforce convexity of subproblem P_{U1}. For the simulated microgrid system, the largest argument in the equation of Theeorem 2.5.1 results from the following DER parameters, $\{R_{fi} = 0.0046p.u., L_{fi} = 0.23p.u., K_i = 0.8, D_i = 0.03528p.u.$ and $\omega = 1p.u.\}$. Substituting these values into the expression of Theorem 2.5.1, we get the lower limit of ρ to

be 1.704. We simulated the system for ρ settings of 10 to 10^4 to obtain the simulation result presented in Fig. 2.12. It is clear that in all cases the residual eventually settles to 0 value, albeit at different rates. This is consistent with the theoretical findings in [43] which states that, ADMM iterates are guaranteed to converge for any positive ρ given the formulation of minimization subproblems is convex. We fixed the ρ to 100 in our optimization problem because it results in the least number of iterations to converge to solution and it allows sufficient slack from lower limit of ρ which is 1.7. Under exceptional circumstances, if the lower bound of ρ is more than this preset value, the new ρ setting is to be broadcasted to all the agents.
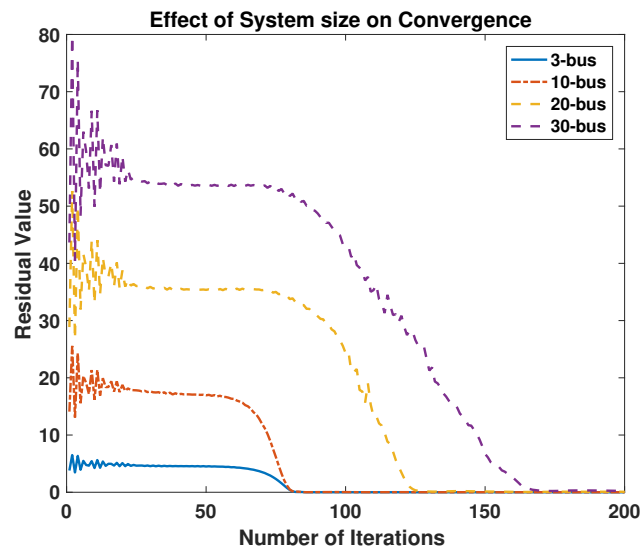
Figure 2.11: Impact of System Size

Feasibility and Adaptability

In this microgrid coordination scheme, we do not adopt loose relaxations to obtain a convex reformulation of the problem like in Ch. 2.4. Therefore, our proposed decentralized algorithm is always expected to recover a feasible solution for any load composition, given that sufficient real and reactive power capacity is available. Recall that, this was not the case for the previous coordination scheme where shunt capacitive compensations were required to obtain an feasible solution for several load compositions. Hence, the current problem reformulation is a certain improvement over the previous coordination scheme which employed non-exact relaxations. To confirm that the proposed scheme guarantees feasibility of the evidently non-convex bus
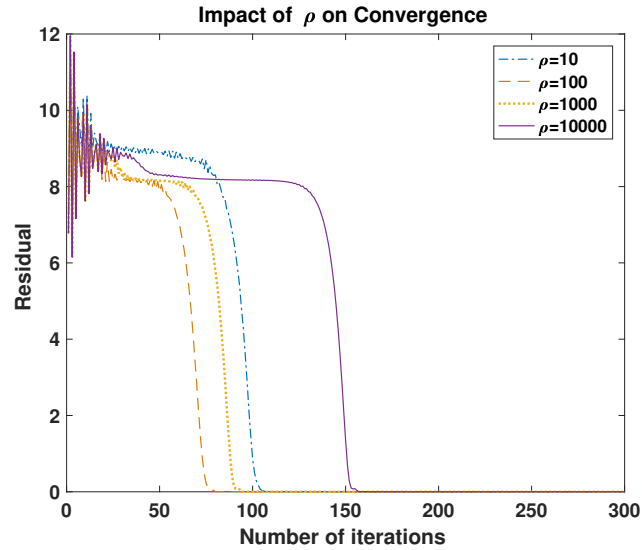
Figure 2.12: Impact of ρ on convergence

voltage constraint for microgrids, we present the bus voltage output in Fig. 2.13 for different degrees of inductive loading in a thirty-bus microgrid system. The bus loading was varied in the range of 1 p.u. to 2 p.u. by mainly changing the RL load parameter in each bus, because the inductive loads have the largest influence in depressing the bus voltage. It can be observed in Fig. 2.13 that the mean bus voltage and its 95% confidence interval are well within the standard acceptable variation of ±5% from the nominal value. Hence, we reaffirm through our simulations that feasibility limits are maintained by the coordination method even under severe system stress.

In Fig. 2.14, we show the overall cost of power in the microgrid for the same range of bus loading. The cost increases almost linearly with the degree of bus loading, as the current injection increases with load. The unit power cost K_i assigned to DER generation for the above simulations are randomly generated positive values.

In certain coordination scenarios, the unavailability of a DER source must be accounted for by increasing the generation from the other available sources based on cost-minimization and feasibility considerations. Our problem formulation deals with the absence or unavailability of a DER from a bus by forcing the corresponding DER injection current state, I_i to 0 using
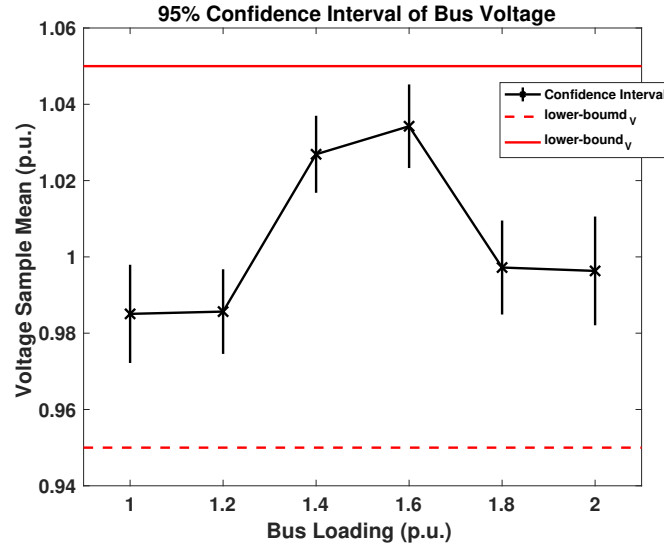
Figure 2.13: Voltage feasibility at bus under changing load
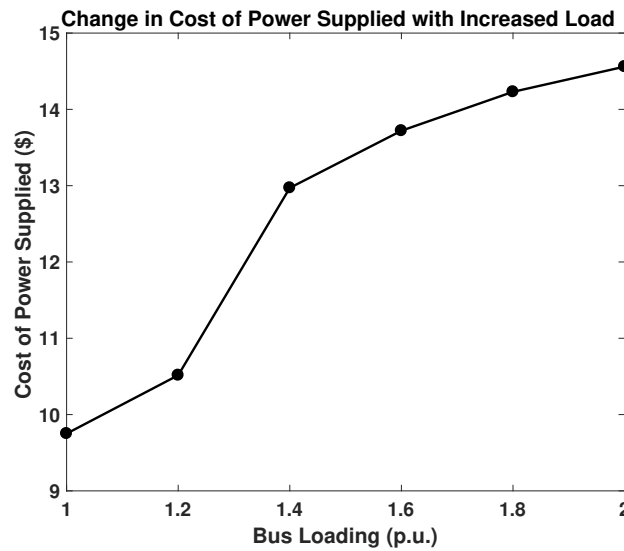
Figure 2.14: Optimal Cost of Power with changing load

constraint ($C5$). The indicator variable, $\mathbb{I}_{empty}(i)$ is set to be 1 if there is no DER associated . In addition to that, constraint ($C2$) is nullified by the product term $(1 - \mathbb{I}_{empty}(i))$ as this equation no longer remains relevant for the particular subsystem. To clearly exhibit the adaptability of the coordination scheme to unavailability of a DER, we first look at the power sharing of the sources in a five-bus microgrid with and without the DER at bus 4, as shown in the first graph of Fig. 2.15. It is evident from the illustration that in the absence of source capacity at a certain node, the other sources re-adjust to maintain the total load consumption and power balance in

the microgrid. The bus voltage feasibility of the microgrid in both scenarios is shown in Fig. 2.16. The recomputation of dispatch set-points is such that the operational constraints of all subsystems and the voltage regulation at the buses can be sustained without the source at bus 4.
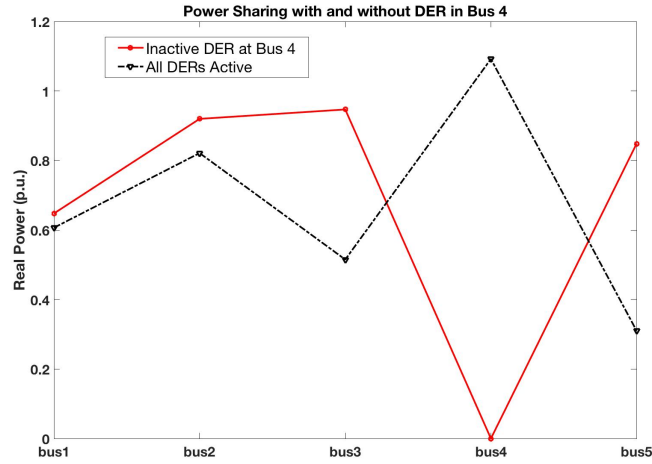
Figure 2.15: Power sharing for inactive DERs
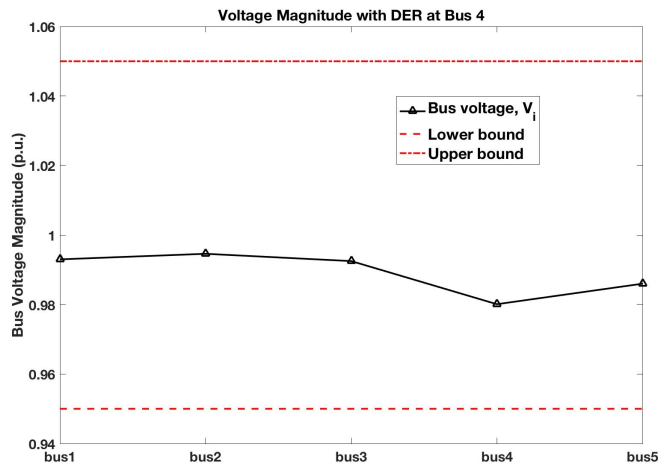
Figure 2.16: Voltage feasibility for inactive DERs

Comparative Studies

Now, we show some essential simulation results to highlight the key differences between the proposed algorithm and some state-of-the-art source dispatch schemes for microgrids. To be

specific, we intend to emphasize the feasibility of the results obtained by our method due to incorporating all fundamental physical constraints which maintain supply-demand balance in an exact manner. The results for the comparison of our decentralized source coordination with an incremental cost-based droop method in [16] is shown in Fig. 2.17. In [16], local measurements are utilized for real-time coordination of sources in a decentralized manner that entails no communication. To achieve almost instantaneous decision making and discard communication, the optimization problem formulated simplifies the calculation of system losses and ignores some critical operational attributes such as reactive power balance. This may cause violation of system limits, when it is not accounted for *exactly* in determining individual source contributions to the microgrid. To prove this, we apply both microgrid optimization method on a five-bus microgrid with the following cost factors for the sources, $\{1000, 1000, 1000, 0.01, 1000\}$. According to the optimization technique proposed in [16], the source at bus 4 meets the power requirements of the entire microgrid when sufficient capacity is available. This however, causes violation of system limits, mainly the voltage deviation limit at multiple buses in the microgrid, shown in Fig. 2.17(b). This can cause damage to the microgrid components and leading to cascading outages. In comparison, our optimization technique formulates the steady state active-reactive power balance and system limits in the problem constraints, which prevents the optimization program to postulate source parameters that can lead to infeasibility. Therefore, as shown in Fig. 2.17, our problem formulation limits contribution of power from bus 4 in order to maintain feasibility across the system.

In table. 2.1, we also compare the performance of our proposal with some existing works in the area of microgrid power sharing. The comparison is based on four essential attributes: 1) Convergence rate 2) Communication overheads 3) Relaxations and 4) Feasibility guarantee. These features essentially define the applications of various coordination schemes based on system requirements, cost considerations, etc. For a system of size n ((i.e. number of nodes/subsystems participating in coordination), the convergence rate is $O(n)$ for decentralized optimization algorithm based on convex formulation like ours and in references [21] and [19]. In a centralized system however, the computational cost of obtaining an optimal solution to the optimization problem is $O(n^3)$. in decentralized coordination algorithms that incorporate
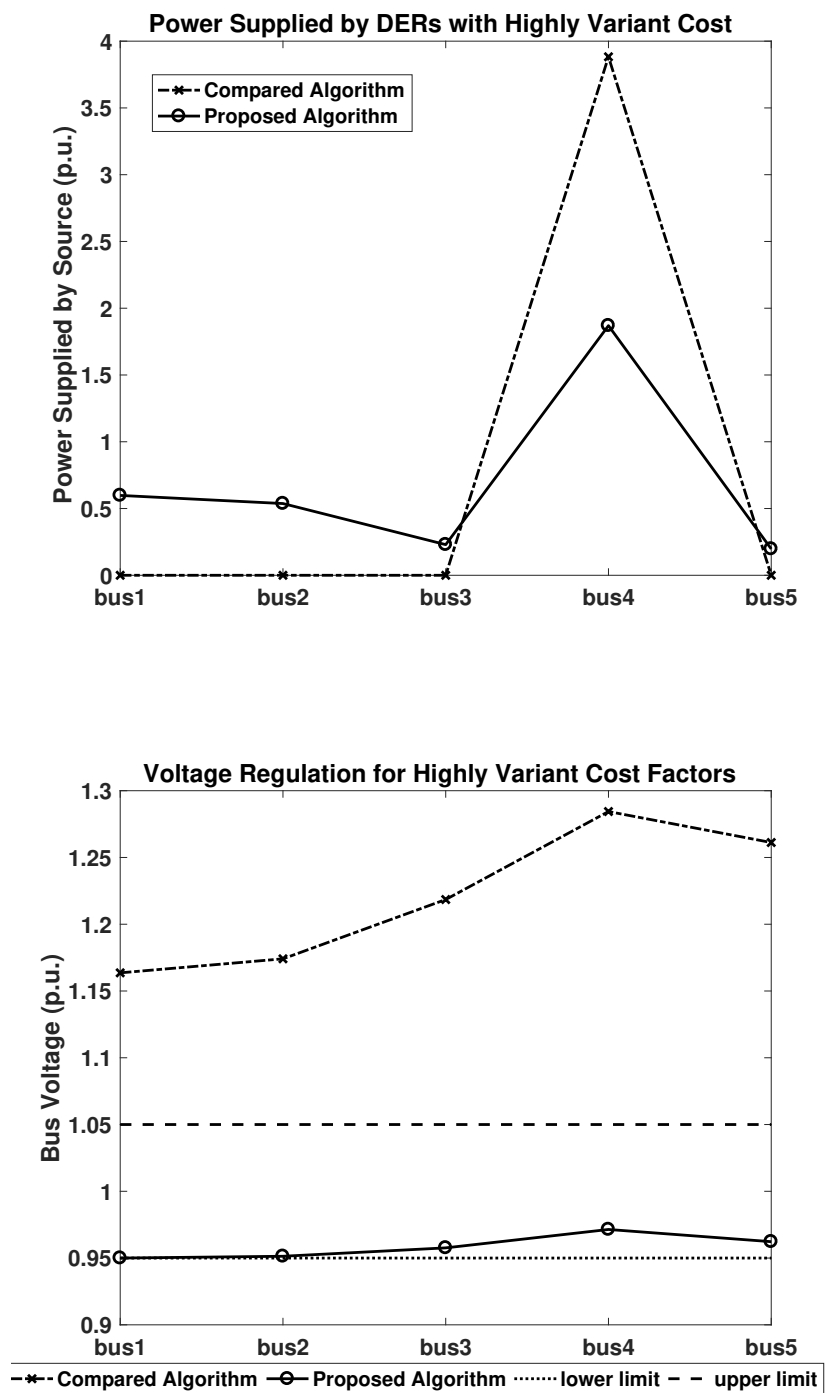
Figure 2.17: (a) Power Sharing (b) Voltage Regulation Capability

only neighbouring peer-to-peer communication, the communication overhead incurred is only $O(m)$, where m is the number of neighbours to a coordinating agent. For decentralized system, the state measurements from all nodes need to be communicated to a single point incurring communication cost of $O(n)$ which is substantially greater and requires a more extensive communication infrastructure. Key relaxations such as rank relaxation or second order cone (SOC) relaxations were applied in references [21] and [19] to obtain a convex formulation much like our non-exact relaxation in Ch. 2.4. References [16] and [40] also ignore the reactive power balance and voltage regulation constraints which can cause infeasibility in the obtained result. Our decentralized coordination algorithm exhibits superior convergence property and guarantees feasibility of the obtained solution due to employing exact convex relaxations. It is therefore well suited for near real-time source coordination for maintaining efficient operation of the microgrid.

	Proposed Algorithm	Incremental-cost droop algorithm [16]	Decentralized OPF algorithm Type 1 [19]	Decentralized OPF Algorithm Type 2 [21]	Centralized Algorithm in [40]
Convergence to optimal point	Linear $O(n)$	-	Linear $O(n)$	Linear $O(n)$	$O(n^3)$
Communication Overhead	$O(m)$	-	$O(m)$	$O(m)$	$O(n)$
Relaxations of physical microgrid constraints	None	Reactive power balance or voltage regulation not considered	SOCP inequality relaxation	Optimal Solution, X^* Rank relaxation	Reactive power balance or voltage regulation not considered
Feasibility in Original OPF	Feasible	Not guaranteed	Not guaranteed	Not guaranteed	Feasible

Table 2.1: Performance Comparison of Proposed Algorithm

Chapter 3

Decentralized Optimization of Source Injection in Distribution Networks

This chapter introduces a novel reformulation of the coordination problem of distributed sources in a radially connected active DN. Our problem formulation is decentralized for every node and employs a convex relaxation that guarantees feasibility of the final solution. The proposed optimization technique is tested on standard IEEE distribution network test systems to examine its applicability for various load and generation scenarios encountered in modern distribution systems.

3.1   System Model

The branch flow model is a set of complex non-linear equations that fully define the operation of a transmission or distribution network. First, the network is considered to be a connected and directed graph $G = (\mathcal{N}, \vec{E})$, where $\mathcal{N}$ is the number of nodes that corresponds to a bus and E contains all directed lines connecting a bus $i \in \mathcal{N}$ to another bus j [54]. All lines are considered to be directed upstream , i.e. towards the substation in a distribution network. The model is based on complex variables such as bus voltage V_i, net power injection s_i, power flowing in line $S_{ij} = P_{ij} + \mathbf{j}Q_{ij}$, and current in the same line I_{ij}, where $i \rightarrow j \in \vec{E}$ is the directed line

between node i and node j. Each line also has a complex impedance $z_{ij} = r_{ij} + \mathbf{j}x_{ij}$. Together these state variables and system parameters characterize a set of power flow equations known as the *Branch Flow Model* (BFM) [54]:

$$\sum_{k:i \to k} S_{ik} = \sum_{j:j \to i} \left(S_{ji} - z_{ji}|I_{ji}|^2 \right) + s_i, \quad i \in \mathcal{N} \tag{3.1}$$

$$I_{ik} = y_{ik}(V_i - V_k), \quad i \to k \in \vec{E} \tag{3.2}$$

$$S_{ik} = V_i I_{ik}^H, \quad i \to k \in \vec{E} \tag{3.3}$$

In the steady-state power flow equations shown above, Eq. 3.1 maintains power balance in each node, Eq. 3.2 is the Ohm's law relation in a particular line and Eq. 3.3 is the formula for line power flowing from bus i to bus k. These equations are normally incorporated as underlying constraints in an OPF problem. The standard method of solving such optimization problems in complex space is to convert it into real-valued problems of real and imaginary parts of the complex arguments. However, this is associated with a high computational complexity and does not overcome any of the nonlinearities in Eq. 3.1-3.3.

If the phase information contained in the complex variables V_i and I_{ij} is discarded, two new real variables defined as $v_i = |V_i|^2$ and $\ell_{ij} = |I_{ij}|^2$ can be obtained. Using these new variables and substituting Eq. 3.3 into Eq. 3.2, we can rewrite Eq. 3.2 as:

$$v_i = v_k + (z_{ik}S_{ik}^* + z_{ik}^*S_{ik}) - |z_{ik}|^2\ell_{ik}$$

Also squaring both sides of Eq. 3.3 we get:

$$v_i\ell_{ik} = |S_{ik}|^2$$

Adopting these equations and separating the real and imaginary parts in Eq. 3.1, we obtain

an equivalent formulation of the branch flow model solely in terms of real variables [55]:

$$\sum_{k:i\to k} P_{ik} = \sum_{j:j\to i} \left(P_{ji} - r_{ji}\ell_{ji} \right) + \mathrm{p}_i, \quad i \in \mathcal{N}$$

$$\sum_{k:i\to k} Q_{ik} = \sum_{j:j\to i} \left(Q_{ji} - x_{ji}\ell_{ji} \right) + \mathrm{q}_i, \quad i \in \mathcal{N}$$

$$v_i = v_k + 2\left(r_{ik}P_{ik} + x_{ik}Q_{ik}\right) - \left(r_{ik}^2 + x_{ik}^2\right)\ell_{ik}, \quad i \to k \in \vec{E}$$

$$v_i \ell_{ik} = P_{ik}^2 + Q_{ik}^2, \quad i \to k \in \vec{E} \tag{3.4}$$

These equations are referred to as the *relaxed branch flow model*. The relaxed BFM was first proposed in the following works [56, 57]. To a power flow optimization problem, the first three lines in Eq. 3.4 are convex linear constraints, while the fourth constraint is a quadratic equality constraint that doesn't comply with the definition of convex sets discussed in Ch. 2.3.1. Therefore, the overall optimization problem based on relaxed BFM is primarily non-convex. Together, the equations in the relaxed BFM define feasible set for variables $\{P_{ij}, Q_{ij}, v_i, l_{ij}, p_i, q_i\}$. During the steady state operation of an electrical system, the actual voltage and line current variables are phasors with phase angles $\angle V_i$, $\angle I_{ij}$. Hence, to accurately model an electrical network using the relaxed BFM model, it is essential that a feasible solution to the equations in terms of transformed real variables correspond to a unique solution in the complex space for the general BFM. This one-to-one correspondence between the solution set of relaxed BFM equations and the complex feasible set defined by the general BFM equations has been proven to hold for radial networks in reference [55]. A decentralized algorithm to recover the phasor values of the state variables from their real valued solution in Eq. 3.4 are also given in reference [55]. Hence, the real domain relaxation of the BFM is sufficient and exact for representation of a radial electrical network in an optimal power flow problem.

3.2   Decentralization and Convex Relaxation

The characteristic configuration of a radial distribution network allows us to disintegrate the optimal power flow problem into subproblems for $\mathcal{N}$ buses in the system. First it must be

recognized that each bus i in the radial network is connected to the rest of the system as shown in Fig. 3.1. Bus i can potentially have multiple branches spanning into downstream nodes, which we refer to as *child* nodes c_i. In contrast, bus i has only one unique line connecting it to a node upstream in the distribution network referred to as *ancestor* node, A_i [19]. The squared magnitude current and the sending-end power in the line between bus i and its ancestor A_i are quantities that are distinct to each bus. Hence, we enlist them as local variables to the bus referred to as l_i and S_i respectively [19]. The impedance of the line between node i and its ancestor is also denoted by z_i. The squared magnitude of bus voltage, v_i and the net power injection into the bus, s_i are also naturally local variables to bus i. These notations are summarized in Table. 3.1.
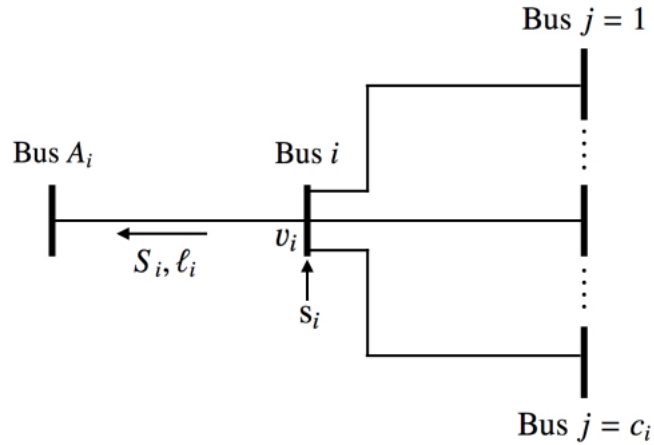
Figure 3.1: Single-line Diagram of Interconnections to Node i in a Radial Network

The exceptions to this generalized form of notations for a bus are the nodes at the ends of the network tree. One node is the *root* node (i.e. the substation bus) which has no ancestor hence, the variables ℓ_i and S_i are void for this node. The root node is unique in a radial distribution network and is identified as bus $i = 1$ of $\mathcal{N}$ buses. Similarly the nodes at the end of the network in downstream do not have any child nodes, c_i. These nodes are also known as *leaf* nodes. In a fully connected radial network, the number of edges $\vec{E} = \mathcal{N} - 1$ [19]. This means all nodes except the root must have a line connecting to ancestor, hence the *edge* set is defined for the given radial network as $\vec{E} = \{2, \ldots, \mathcal{N}\}$.

Notations for bus i	
c_i	Child nodes to i
A_i	Ancestor node of i
v_i	Squared bus voltage
ℓ_i	Current in line $i \rightarrow A_i$
$s_i = p_i + \mathbf{j}\, q_i$	Net power injection at bus i
$S_i = P_i + \mathbf{j}\, Q_i$	Sending end power in line $i \rightarrow A_i$
$z_i = r_i + \mathbf{j}\, x_i$	complex impedance in line $i \rightarrow A_i$

Table 3.1: Summary of Notations for bus i

Using the aforementioned notations, the optimal power flow problem of the active distribution network is formulated as follows:-

$$\mathcal{P}_{AC} : \underset{S_i, v_i, \ell_i, s_i}{\text{minimize}} \sum_{i \in \mathcal{N}} f_i(\mathrm{p}_i)$$

subject to:

$$s_i \in \mathcal{I}_i, \quad \forall i \in \mathcal{N} \tag{C1}$$

$$P_i = \sum_{\forall j \in c_i} \left(P_j - r_j \ell_j \right) + \mathrm{p}_i, \quad \forall i \in \mathcal{N} \tag{C2}$$

$$Q_i = \sum_{\forall j \in c_i} \left(Q_j - r_j \ell_j \right) + \mathrm{q}_i, \quad \forall i \in \mathcal{N} \tag{C3}$$

$$v_i = v_{A_i} + 2\left(r_i P_i + x_i Q_i \right) - (r_i^2 + x_i^2)\ell_i, \quad \forall i \in \vec{E} \tag{C4}$$

$$0.95^2 \leq v_i \leq 1.05^2, \quad \forall i \in \mathcal{N} \tag{C5}$$

$$P_i^2 + Q_i^2 - v_i \ell_i \leq 0, \quad \forall i \in \vec{E} \tag{C6}$$

$$P_i^2 + Q_i^2 - v_i \ell_i \geq 0, \quad \forall i \in \vec{E} \tag{C7}$$

Each source in the network will inject power at a particular bus i according to its feasible injection region, $\mathcal{I}_i$ which depends on the capacity of the energy source and controllability of the interfacing power electronic converter [58]. These can be approximated as box constraints specifying limits on the real and reactive power injected by a source. Finally, a binary variable $\mathbb{I}_S(i)$ indicates the availability of a source for coordination at bus i. Together these conditions

define the feasible injection region in constraint $(C1)$ of source at bus i as follows:-

$$\underline{s_{Gi}} \leq s_{Gi} \leq \overline{s_{Gi}}$$

$$s_i = s_{Gi} - s_{Li}$$

$$\mathbb{I}_S(i) \, s_{Gi} = 0$$

where s_{Gi} is the generation and s_{Li} is the load at any bus i. When the power flow problem is formulated to minimize the cost of DG power in the microgrid, the cost function typically appears as a quadratic function of the generated power of DGs : $\alpha_i P_{Gi}^2$. This cost factor can be set by the independent producer to recover costs of investment, operation and maintenance or it can be assigned by market entities depending on market signals [50]. This will facilitate peer-to-peer energy trading in smart grids which is becoming highly plausible due to advent of technologies such as Blockchain [4].

The constraints $(C2) - (C6)$ in $\mathcal{P}_{AC}$ are the relaxed BFM equations for a radial network in terms of the notations summarized in Table. 3.1. Among these, constraints $(C2)$ and $(C3)$ are formed to maintain power balance for every bus, i for all $i \in \mathcal{N}$. The constraint (C4) is the squared Ohm's law relation signifying magnitude of voltage drop due to power flow in the line between bus i and its ancestor A_i. Constraint $(C5)$ limits the bus voltage deviation to ±5% from nominal value. Finally, the quadratic equality constraint associated with the line power flowing out of bus i is represented as a combination of two inequality constraints $(C6)$ & $(C7)$ as outlined in reference [53]. $(C6)$ is a convex second order cone relaxation for the line power which in certain scenarios is independently sufficient to obtain the same result as the quadratic equality [10]. Operational conditions under which this stands true has been outlined in reference [59]. However, feasibility of the original constraint can be violated in that method for some anticipated scenarios in active distribution networks (e.g. bidirectional power flow in the lines). For a more comprehensive representation of the relaxed BFM, the inequality $(C7)$ must be incorporated in the optimization problem $\mathcal{P}_{AC}$ to exactly account for the quadratic equality constraint associated with line power, $i \to A_i$. It can be easily deciphered from their respective equations that the set defined by constrain $(C7)$ is the *absolute complement* of the convex set defined by $(C6)$ (formal definition: Absolute complement of *set* $A = \{x \in U \,|x \notin$

A}). This implies that as the set defined by constraint ($C6$) is convex, the set defined by its absolute complement constraint ($C7$) is non-convex which therefore results in non-convexity of problem $\mathcal{P}_{AC}$.

The problem $\mathcal{P}_{AC}$ is not separable for a bus i because of the power balance constraints ($C2$)-($C3$) and the constraint pertaining to voltage drop and current flow in $i \rightarrow A_i$ line, ($C4$). These constraints are composed of variables which inherently belong to the child nodes, c_i or ancestor node, A_i. Moreover, the localized non-convex constraint ($C7$) renders the problem NP-hard which implies that the problem is not solvable in polynomial time [60]. The problem $\mathcal{P}_{AC}$ can be attempted to be solved by a central agent to determine the power injection set points for the sources. However, this is not scalable for a NP-hard problem in modern electrical networks with numerous intelligent nodes that needs to be simultaneously optimized. Therefore, we propose a decentralized optimization algorithm leveraging the decomposability of ADMM simiar to Ch. 2.3.2 to construct an equivalent form of $\mathcal{P}_{AC}$ which is convex and separable for every intelligent node.

To achieve this objective, first it is required that every agent decomposes the problem between two sets of variables: local and perspective variables [19]. The local variables for a particular bus are similar to those defined in Table 3.1 of the previous section, but we add a superscript x to the variables to distinguish them as local variables. Perspective variables y_i considered for this problem are basically local perspectives of specific variables in local bus, i and neighbouring buses, c_i or A_i. Perspective variables, y_i allow us to formulate the non-separable constraints (i.e. incorporates non-local variables) in P_{AC} in terms of locally solved states. The general form of these variables for a bus i in the network is shown below:

$$x_i = \{P_i^x, Q_i^x, v_i^x, \ell_i^x, \mathrm{p}_i^x, \mathrm{q}_i^x\}$$

$$y_i = \{P_{i,i}^y, Q_{i,i}^y, v_{i,i}^y, \ell_{i,i}^y, \mathrm{p}_{i,i}^y, \mathrm{q}_{i,i}^y, v_{Ai,i}^y, P_{j,i}^y, Q_{j,i}^y, \ell_{i,i}^y \; \forall j \in c_i\} \tag{3.5}$$

In the perspective variables, the first term in the subscript denotes perspective of and the second term denotes perspective from. For example, $P_{j,i}^y$ is the perspective of local branch real power in bus j from the perspective of bus i. The perspective variables y_i are solved for such

that they belong to the feasible set, $\mathcal{Y}_i$ defined by the following equations:

$$s^y_{i,i} \in \mathcal{I}_i, \tag{C1}$$

$$P^y_{i,i} = \sum_{\forall j \in c_i} \left(P^y_{j,i} - r_j \ell^y_{j,i} \right) + p^y_{i,i} \tag{C2}$$

$$Q^y_{i,i} = \sum_{\forall j \in c_i} \left(Q^y_{j,i} - r_j \ell^y_{j,i} \right) + q^y_{i,i} \tag{C3}$$

$$v^y_{i,i} = v^y_{A_i,i} + 2 \left(r_i P^y_{i,i} + x_i Q^y_{i,i} \right) - (r_i^2 + x_i^2) \ell^y_{i,i} \tag{C4}$$

$$0.95^2 \le v^y_{i,i} \le 1.05^2 \tag{C5}$$

$$(P^y_{i,i})^2 + (Q^y_{i,i})^2 - v^y_{i,i} \ell^y_{i,i} \le 0 \tag{C6}$$

Therefore, the feasible set $\mathcal{Y}_i$ is a convex set defined by the convex constraints (C1)-(C6). The purpose of maintaining perspective variables of certain neighbouring states (e.g. $P^y_{j,i}, Q^y_{j,i}, \dots$) is revealed by the formulation of the above feasible set, $\mathcal{Y}_i$. The program uses these variables to implement local representation of constraints that are inherently non-separable for a certain bus. Having defined $\mathcal{Y}_i$ as such, the non-convex constraint (C7) has been isolated which shall thereby define another feasible set, $\mathcal{X}_i$. We solve for the local variables, x_i to belong to this feasible set $\mathcal{X}_i$ and rewrite constraint (C7) in terms of x_i:

$$(P^x_i)^2 + (Q^x_i)^2 - v^x_i \ell^x_i \ge 0 \tag{C7}$$

To ensure that the variables x_i and y_i eventually satisfy all constraints of problem $\mathcal{P}_{AC}$, consensus must be enforced between the local and perspective variables. This is achieved by incorporating the consensus condition as a constraint to formulate an ADMM based decom-

posed optimization problem as shown:

$$\mathcal{P}_D : \operatorname*{minimize}_{x_i \in \mathcal{X}_i, y_i \in \mathcal{Y}_i} \sum_{i \in \mathcal{N}} f_i(\mathrm{p}_i^x)$$

$$\text{subject to: } \forall i \in \mathcal{N}$$

$$P_i^x = P_{i,i}^y \,, Q_i^x = Q_{i,i}^y \,, v_i^x = v_{i,i}^y \,, \ell_i^x = \ell_{i,i}^y \,, \mathrm{p}_i^x = \mathrm{p}_{i,i}^y \,, \mathrm{q}_i^x = \mathrm{q}_{i,i}^y \,,$$

$$P_i^x = P_{i,Ai}^y \,, Q_i^x = Q_{i,Ai}^y \,, \ell_i^x = \ell_{i,Ai}^y \,,$$

$$v_i^x = v_{i,j}^y \qquad \forall j \in c_i$$

Due to the consensus constraints, every perspective variable is compelled to be equal to their actual states in local or neighbouring buses. The optimization problems $\mathcal{P}_D$ and $\mathcal{P}_{AC}$ are equivalent when the consensus constraints are satisfied. Like in Ch. 2.3.2, the consensus constraints of $\mathcal{P}_D$ are represented hereon as $Mx - Ny = 0$. The augmented Lagrangian function for problem $\mathcal{P}_D$ is thus constructed as follows:

$$
\begin{aligned}
\mathcal{L}_\rho^D(x, y, v) &= \sum_{i \in \mathcal{N}} f_i(x_i) + v^T (Mx - Ny) + \frac{\rho}{2} \|Mx - Ny\|_2^2 \\
&= \sum_{i \in \mathcal{N}} \Big[f_i(\mathrm{p}_i^x) + v_{i,i}^P (P_i^x - P_{i,i}^y) + v_{i,i}^Q (Q_i^x - Q_{i,i}^y) + v_{i,i}^v (v_i^x - v_{i,i}^y) + v_{i,i}^\ell (\ell_i^x - \ell_{i,i}^y) \\
&\quad + v_{i,i}^\mathrm{p} (\mathrm{p}_i^x - \mathrm{p}_{i,i}^y) + v_{i,i}^\mathrm{q} (\mathrm{q}_i^x - \mathrm{q}_{i,i}^y) + \sum_{\forall j \in c_i} \Big\{ v_{j,i}^P (P_j^x - P_{j,i}^y) + v_{j,i}^Q (Q_j^x - Q_{j,i}^y) + v_{j,i}^\ell (\ell_j^x - \ell_{j,i}^y) \Big\} \\
&\quad + v_{Ai,i}^v (v_{Ai}^x - v_{Ai,i}^y) + \frac{\rho}{2} (P_i^x - P_{i,i}^y)^2 + \frac{\rho}{2} (Q_i^x - Q_{i,i}^y)^2 + \frac{\rho}{2} (v_i^x - v_{i,i}^y)^2 + \frac{\rho}{2} (\ell_i^x - \ell_{i,i}^y)^2 \\
&\quad + \frac{\rho}{2} (\mathrm{p}_i^x - \mathrm{p}_{i,i}^y)^2 + \frac{\rho}{2} (\mathrm{q}_i^x - \mathrm{q}_{i,i}^y)^2 + \sum_{\forall j \in c_i} \Big\{ \frac{\rho}{2} (P_j^x - P_{j,i}^y)^2 + \frac{\rho}{2} (Q_j^x - Q_{j,i}^y)^2 + \frac{\rho}{2} (\ell_j^x - \ell_{j,i}^y)^2 \Big\} \\
&\quad + \frac{\rho}{2} (v_{Ai}^x - v_{Ai,i}^y)^2 \Big]
\end{aligned}
\tag{3.6}
$$

where v is the dual variable associated with the consensus constraint in $\mathcal{P}_D$ and the dual step size, ρ is set to a value greater than 0 to ensure convergence of the problem [43]. The augmented Lagrangian function, $\mathcal{L}_p^D(x_i, y_i, v_i)$ is dependent simultaneously on the variables x, y and v. We traverse the problem, $\mathcal{L}_p^D$ by dividing it into separate subproblems which independently solve for x and y within feasible sets $\mathcal{X}_i$ and $\mathcal{Y}_i$ in an iterative manner, and

updates v after each iteration based on the difference between local and perspective variables ($Mx - Ny = 0$). The three steps involved in the process of solving the Lagrangian, similar to those in Ch. 2.3.2 are presented below:

$$x_i^{k+1} = \underset{x_i \in X_i}{\operatorname{argmin}} \mathcal{L}_p^S(x, y^k, v^k) \qquad\qquad (U1)$$

$$y_i^{k+1} = \underset{y_i \in Y_i}{\operatorname{argmin}} \mathcal{L}_p^S(x^{k+1}, y, v^k) \qquad\qquad (U2)$$

$$v_i^{k+1} = v_i^k + \rho(Mx^{k+1} - Ny^{k+1}) \qquad\qquad (U3)$$

Superscript $k + 1$ on variables signifies values computed in current iteration and superscript k signifies values computed during the previous iteration, which is held constant during the current iteration. It can be observed from the Lagrangian of problem $\mathcal{P}_D$ shown in Eq. 3.6 that the x and y minimization subproblems, ($U1$) and ($U2$) are separable for each node i, when the values of the other two variables are kept fixed to their previous updates [61]. Communication is required between neighbouring nodes before each step to exchange essential variables required to compute the consensus gap, ($Mx - Ny$) = 0. A generalized communication framework established between a bus i and its neighbouring nodes to facilitate decentralization of the problem is shown in Fig. 3.2.
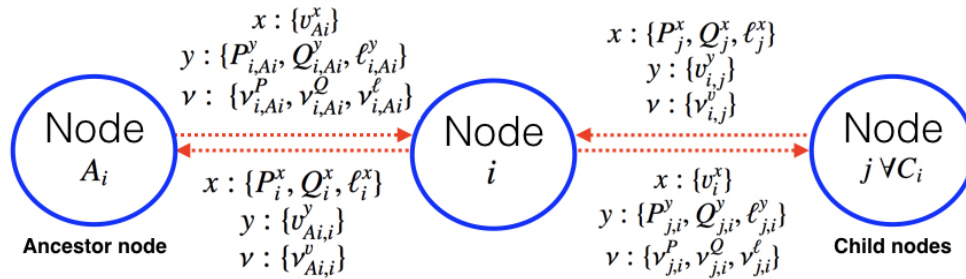
Figure 3.2: General communication framework for bus i

Prior to update ($U1$) in $(k+1)-th$ iteration, the updated values of certain variables in v^k are communicated to bus i and held fixed while solving the subproblem. Similarly before updates ($U2$) and ($U3$), some variables of x^{k+1} and y^{k+1} are communicated to bus i successively. The update variables of $\{x, y, v\}$ that are exchanged between neighbouring nodes to carry out the

decentralized iterative process of solving $\mathcal{P}_D$ are specified in Fig. 3.2 from the perspective of a certain bus i in the system.

The procedure to attain convergence of solutions x_i and y_i by iterating through the steps $(U1)$-$(U3)$ is already outlined in Alg. 1 of ch. 2.3.2. For the ADMM problem $\mathcal{P}_D$ to converge, it is imperative that the respective subproblems $(U1)$ and $(U2)$ have convex forms so that x and y variables can be iteratively minimized. Subproblem $(U2)$ comprises constraints $(C1)$-$(C6)$ of problem $\mathcal{P}_{AC}$ which are convex. The objective of the subproblem is also a convex function as it consists of pure-quadratic terms (i.e $v_{i,i}^{y}{}^2, \ell_{i,i}^{y}{}^2$,etc.) with positive coefficients ρ from the augmented Lagrangian. Hence, subproblem $(U2)$ can be solved optimally at each iteration. In contrast, obtaining an exact solution from subproblem $(U1)$ is not as straightforward because the solution, x^{k+1} lies in a set defined by constraint $(C7)$ which is non-convex.

The general form of subproblem $(U1)$ is shown below in terms of coefficient matrices resulting from the augmented Lagrangian function in Eq. 3.6 and the constraint $(C7)$:

$$\mathcal{P}_{U1}^i : \quad \underset{x_i \in X_i}{\text{minimize}} \quad \frac{1}{2} x_i^T \left(A_0^i + B_0^i \right) x_i \; + \; C_0^i \, x_i$$

$$s.t. \; 0 \leq \frac{1}{2} x_i^T A_1^i x_i$$

$$\text{where, } A_1^i = 2 \cdot \begin{bmatrix} 1 & 0 & 0 & 0 & \cdots \\ 0 & 1 & 0 & 0 & \\ 0 & 0 & 0 & \frac{-1}{2} & \\ 0 & 0 & \frac{-1}{2} & 0 & \\ \vdots & & & & \ddots \end{bmatrix} \tag{3.7}$$

There are crucial differences between the above formulation and the subproblem $\mathcal{P}_{U1}$ defined in Ch. 2.5 for the islanded microgrid problem in a DQ frame of reference. Firstly, the matrix A_0^i in the objective arises from the cost function of the original problem $\mathcal{P}_{AC}$ which is now expressed in terms of x_i within subproblem $\mathcal{P}_{U1}$. The cost function of $\mathcal{P}_{AC}$ has already been defined as $\alpha_i P_{Gi}^2$ earlier. Power p_{Gi} is an optimization variable in this problem, unlike the state-space model based problem P_{OC} in Ch. 2.5 for which generated power had to be expressed as a quadratic function of input voltage and bus voltage, $f(V_{ti}, V_i)$. The cost function, $\alpha_i P_{Gi}$ and

resultantly the term $x_i^T A_0^i x_i$ in objective is certainly convex, for any cost factor α_i which always has a positive value. The other matrices in objective, B_0 and C_0 are similar in characteristic to the previous problem shown in Ch. 2.5. It is important to note that since $x_i^T A_0^i x_i$ is always convex in this problem, there is no restriction on the value of penalty parameter ρ, whereas in Ch. 2.5 the value of ρ was bounded by Theorem 2.5.1. Lastly, the coefficient matrix A_1^i has a more complex form containing off-diagonal elements due to the form of quadratic inequality constraint $(C7)$. Only the relevant block of matrix of matrix A_1^i is shown in the diagram, as the remaining elements in the matrix are 0.

Following the same approach as Ch. 2.5 that utilizes dual function and Schur's complement, we can construct the dual semi-definite program (SDP) , S_{U1} of the problem $\mathcal{P}_{U1}$ as shown below:

$$\mathcal{S}_{U1} : \underset{\lambda, \gamma}{\text{maximize}} \quad \gamma$$

$$s.t. \ \lambda \geq 0$$

$$\begin{bmatrix} A_0 + B_0 - \lambda A_1 & C_0 \\ C_0^T & -\gamma \end{bmatrix} \geq 0$$

This concave dual problem is then solved to obtain the dual optimal λ^*. Strong duality holds between the corresponding dual optimal value g^* and the optimal value of the primal problem, $\mathcal{P}_{U1}^*$. This is because the problem $\mathcal{P}_{U1}$ belongs to the same special case of quadratically constrained quadratic program (QCQP) described in Theorem 2.5.2 for which the dual program holds strong result (i.e. $g^* = \mathcal{P}_{U1}^*$) [42]. Hence, according to the theory of S-procedure, the primal optimal solution, $(x)^{k+1}$ in a specific iteration can be obtained for subproblem (U1) by directly substituting λ^* into the following closed-form expression obtained using the first order optimality condition $\frac{\partial \mathcal{L}_{U1}}{\partial x} = 0$, where $\mathcal{L}_{U1}$ is the Lagrangian function of problem $\mathcal{P}_{U1}$:

$$\frac{\partial \mathcal{L}_{U1}}{\partial x} = (A_0 + B_0) x + C_0 - \lambda (A_1 x) = 0; \tag{3.8}$$

$$x = -(A_0 + B_0 - \lambda A_1)^{-1} (C_0) \tag{3.9}$$

Applying the aforementioned techniques, the decentralized optimization algorithm solves the subproblems ($U1$) and ($U2$) at every iteration. The ADMM iterates eventually converge to the final solution x' for a given coordination event, when the residual $\|Mx - Ny\|_2^2$ falls below threshold ϵ in Alg. 1 of Ch. 2.5. At this stage the terms $v(Mx - Ny)$ and $\frac{\rho}{2}\|(Mx - Ny)\|_2^2$ in Eq. 3.6 tends to 0, which means the Lagrangian function reduces to the objective in problem, $\mathcal{P}_D$. This implies that x' and y' are solutions of the optimization problem formulated in $\mathcal{P}_D$, and consequently it is also a feasible solution to the original optimization problem of the active distribution network, i.e. $\mathcal{P}_{AC}$, as it satisfies the consensus constraints.

3.3   Results

The aforementioned optimization algorithm has been applied on 8 bus, 33 bus and 64 bus distribution system parameters [56, 63]. Most of the results presented are obtained for an IEEE-33 bus system with sources distributed across the network as shown in Fig. 3.3. Convergence, feasibility and cost of the proposed solution are analyzed to ascertain key performance attributes of the ADMM based decentralized optimization. Comparison with a state-of-the-art power sharing technique is also presented in this section to highlight improvements over the existing literature.
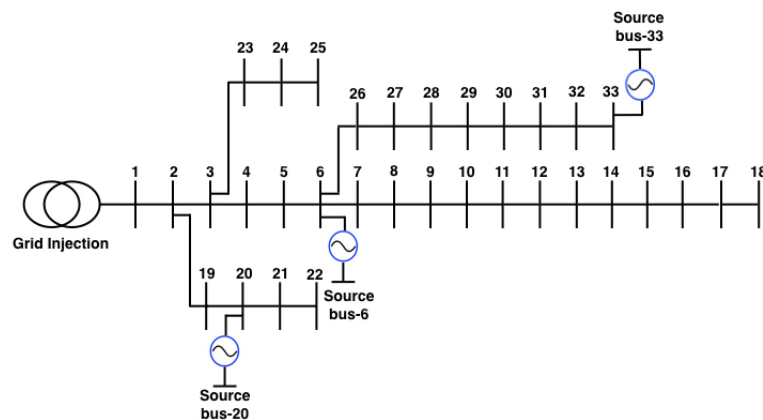

Figure 3.3: Placement of sources in the standard IEEE 33-bus DN

Convergence Study

The progressive decay of the ADMM residual with the number of iterations shown in Fig. 3.4 is obtained by applying the decentralized algorithm on three distribution systems of different sizes. The 8-bus system is a subset of the IEEE 33 bus system which was adopted for initial testing purposes. The other two network parameters utilized for this study are from the IEEE 33-bus and 64-bus distribution systems data. The convergence characteristics of this optimization problem is significantly different from that shown in Ch. 2.5.2 because of the differences in problem dimension and complexity of the problem. The branch flow model contains less constraints leading to lower complexity of the subproblems compared to the state-space model in DQ frame. Furthermore, the objective of the problem to incorporate microgrid cost is a convex quadratic function in this model. It can be observed from Fig. 3.4 that the initially sharp drop in residual occurs within 3 iterations for all three system sizes. Following that, the residual drops at a slower rate to ϵ when there is a larger number of independent coordinating agents (i.e. buses) in the system. This is highlighted by magnifying the portion between iterations 20 to 30 in Fig. 3.4. The residual of convergence for a larger system is seen to be slightly greater at the same number of iterations. Therefore, to converge to the same residual thresold of ϵ the DN with 64 buses will take a higher number of iterations than the 33-bus system or the 8-bus system. The number of iterations required for the IEEE 64 bus DN to attain acceptable convergence was determined to be 200 iterations. Assuming that the cyber elements and communication protocol employed in this coordination method are similar to those in ch. 2.2, the total communication and computational delay incurred in one iteration of the optimization process is about 300ms. This implies that a single coordination event requires about $0.3 * 200 \approx 60s$ to generate the power dispatch set-points. The relatively faster convergence rate compared to the problem in Ch. 2.5 can be attributed to the conceded granularity of the dispatch set-points. For example, this optimization technique only renders the real and reactive power allocation set-points which needs to be further tracked to corresponding voltage set-points by the internal control loops of the inverter. In contrast, the system model of the previous problem enabled us to obtain the exact voltage set-point from the optimization problem itself. Hence, this establishes an essential trade-off between the two proposed models for

microgrid coordination.
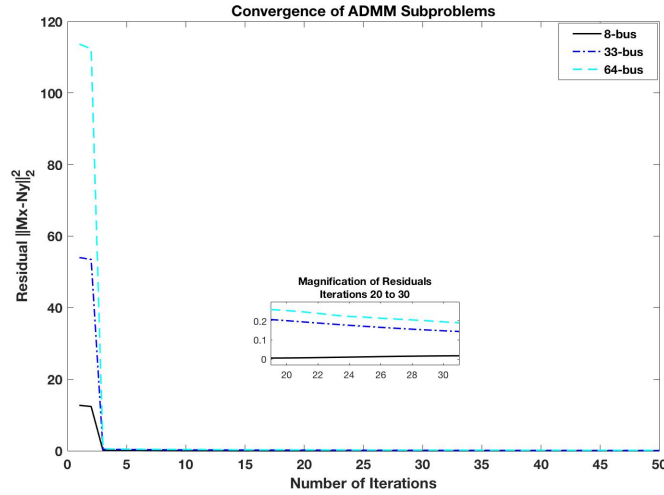
Figure 3.4: Convergence of *x* and *y* variables in ADMM subproblems

Power Sharing Trend

There are 3 distributed sources in our 33-bus system placed at bus 6, 20 and 33, while the grid injection has throughout been modelled as a source at bus 1. The real and reactive power capacity of the sources are given in Appendix C. The objective of our optimization problem tends to minimize the cost of power injection from the sources, which is dependent on the cost factor, α_i. Intuitively, when the cost factor of a particular source is significantly lower, most of the power should be supplied from that source given that the underlying feasibility constraints are met. To demonstrate this, we run the optimization program for five different cost combinations of the 4 power sources. For first four cost combinations, $cost\ 1-4$ in Fig. 3.5 the cost factors, α_i of sources at buses 1, 6, 20 and 33 are set to 1 subsequently, while fixing the remaining cost factors to 8. For example, cost2 has the following cost factors for the respective bus sources {source $bus1 = 8$, source $bus6 = 1$, source $bus20 = 8$, source $bus33 = 8$}. All cost combinations are listed in detail in Appendix C. It can be observed from Fig. 3.5 that the sources with the lower cost factor, α_i supplies the most power in all the different combinations which is expected. The contribution of source at bus 6 is typically high because it is at a strategically superior position in the network (i.e. close to most loads). Therefore, for $cost2$

in Fig. 3.5, the minimum cost solution is reached with almost no power contribution from the other sources because this allocations leads to lower losses while ensuring a feasible solution. For the final cost combination, $cost5$, all sources are assigned a cost factor of 8 which leads to almost equal power sharing among the sources.
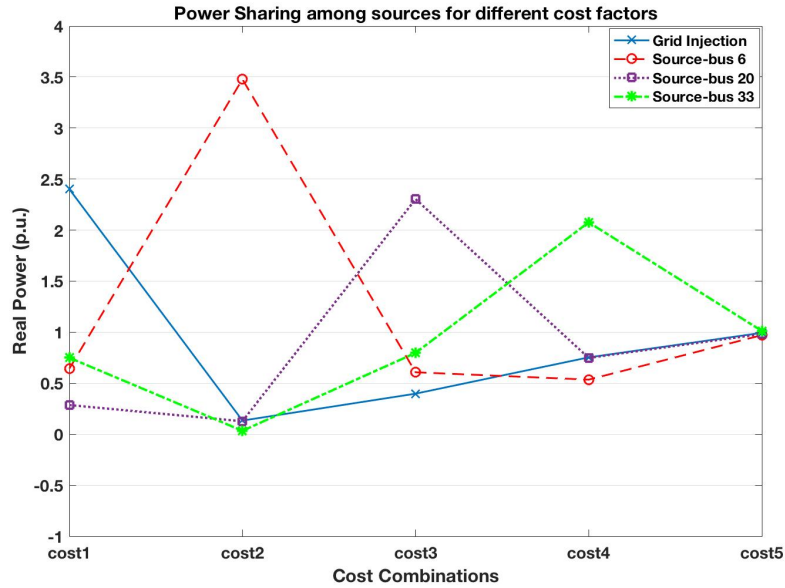
Figure 3.5: Effect of cost factors on power sharing

Next, it is shown in Fig. 3.6 how the distribution and size of loads affect the power allocation of the sources. Keeping cost factors α_i of sources at bus 1, 6, 20 and 33 fixed to $\{2, 5, 3, 9\}$ respectively, the optimization program is run in 4 different load scenarios shown as *load settings* $1 - 4$ in Fig. 3.6. The bus-by-bus load parameters for the load settings are given in Appendix C. For Load Setting 1, the real and reactive load parameters are used verbatim from the IEEE 33-bus DN data. The power sharing in this case is typical depending on their relative cost factors, where maximum power is being injected by the grid due to lower price. In Load Setting 2, the real power demand is adjusted such that it is concentrated towards buses which are close to source bus 6 and 33, while keeping the total real power demand over the whole DN same as before. This leads to an increase in power supplied by sources at bus 6 and 33 due to loss considerations of supplying power from more distant sources. For the case of Load Setting 3, we keep the real power demand at the buses same as *LoadSetting*1 but inflate the reactive power demand to two times at all buses. This will expectedly increase the losses in

the lines, but does not considerably affect power sharing unless voltage feasibility condition is violated. Finally, in Load Setting 4 scenario the real power demand is 2 times and the reactive power demand is 1.5 times that of load setting 1 at every bus. This scenario exhibits how the system reallocates source injection such that the system limits (such as voltage bounds) are not violated under severe system stress. Under this condition, the power supplied by source at bus 6 increases more than that by the other sources although it has a relatively higher cost than some of the other sources. This prevents violation of voltage bounds because loads are being supplied from closest sources given that capacity is available, thereby minimizing voltage drops in the tie lines. The aggregate power supply and demand in the system is also shown in Fig. 3.7 for the discussed load scenarios. The differences between the supply and demand represents the losses in the distribution line.
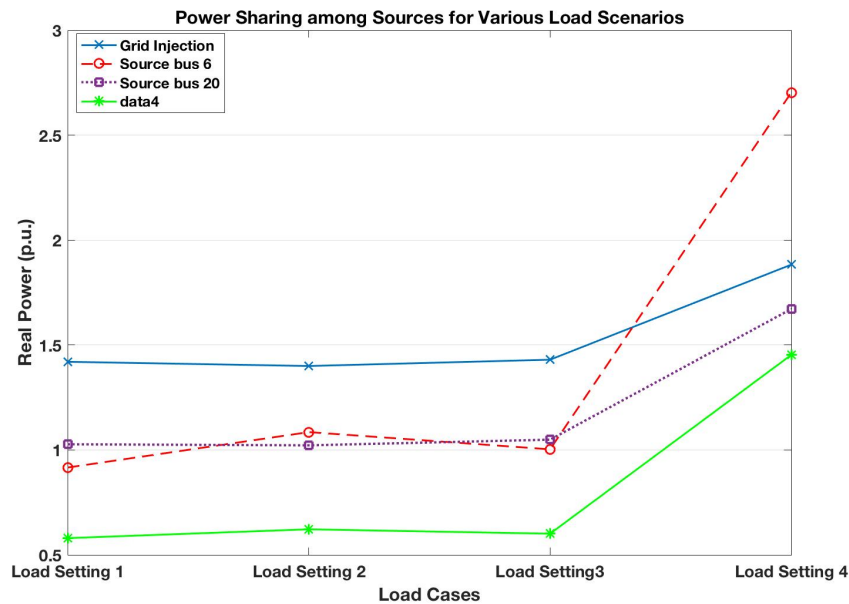
Figure 3.6: Effect of system load on power sharing
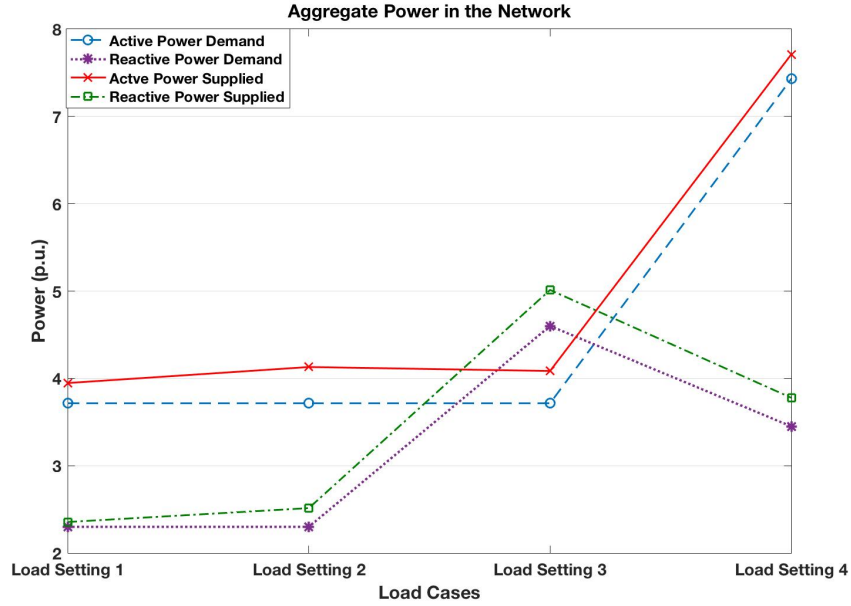
Figure 3.7: Aggregate load-supply in the network

Feasibility and Cost

During steady-state operation, the standard voltage limits of ±5% must be strictly met for sustainable operation of the distribution network. The bus voltages in the final minimum-cost solution, x' is maintained within the feasible region between the red lines in Fig. 3.8 by the voltage regulation constraint ($C5$) in the problem $\mathcal{P}_{AC}$. Some existing optimization techniques such as that in reference [10] omits the voltage upper bound constraint to obtain a convex and exact relaxation to the OPF problem. However, in such cases the solution of the relaxed problem might stray out of feasible region, especially under high system stress like in Load Setting 4 scenario. In contrast, the solution offered by our optimization algorithm is guaranteed to be within the feasible voltage bounds, whenever a feasible solution exists. In Fig. 3.8, the variation in bus voltage magnitude is very low for Load Settings 1 and 2 because these are nominal load conditions. For Load Settings 3 and Load Setting 4, the inflated reactive power demand in the system leads to greater variation between the bus voltages, which is symbolized by the larger interval bars in these load scenarios. The excessively high real power demand in Load Setting 4 also leads to a higher mean bus voltage in the network.

The minimum costs obtained for load settings 1-4 are shown next in Fig. 3.9. Cost is
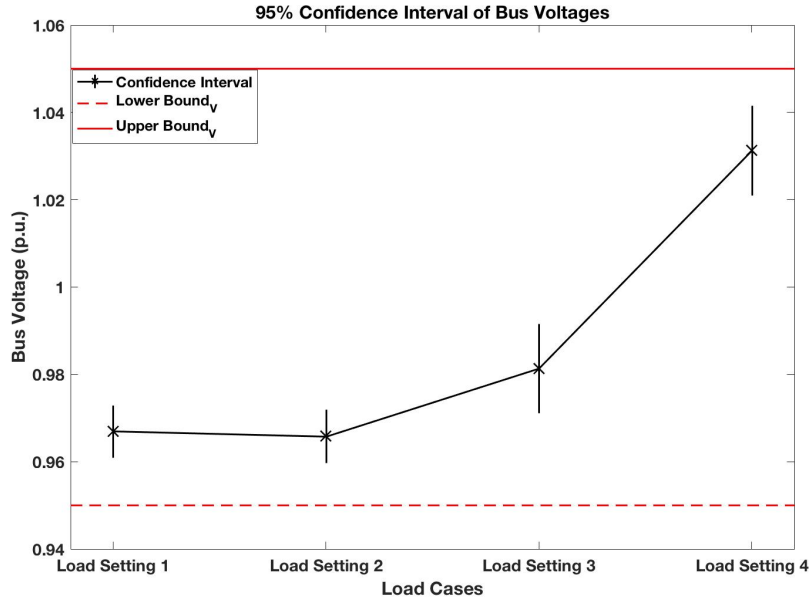
Figure 3.8: Feasibility of bus voltages

dependent on real power supplied by the sources, hence it changes very little between load settings 1-3. This insubstantial change can be attributed to small variations in power allocation and system losses which were already shown in Fig. 3.6 and 3.7 respectively. The cost then increases to a much higher value in load setting 4 which is more than twice the previous costs. This is because more power is being drawn from source at bus 6 in this scenario under feasibility considerations. This source is associated with a higher cost factor which therefore, leads to a larger increase in cost compared to the increase in power supplied.

Comparative Studies

Finally, proof of feasibility guarantee of our proposed algorithm is presented in comparison with a state-of-the-art incremental-cost droop based power sharing scheme presented in reference [16]. In [16], the cost of power supply is minimized while accounting for real power balance in the system. This is a decentralized scheme with no communication entailed which renders rapid convergence. However, this scheme ignores the reactive power balance, exact system losses and voltage bound constraints that are naturally imposed on the system. To exhibit that this can result in infeasible solution, we vary the cost of source at bus 33, α_{33} from 100
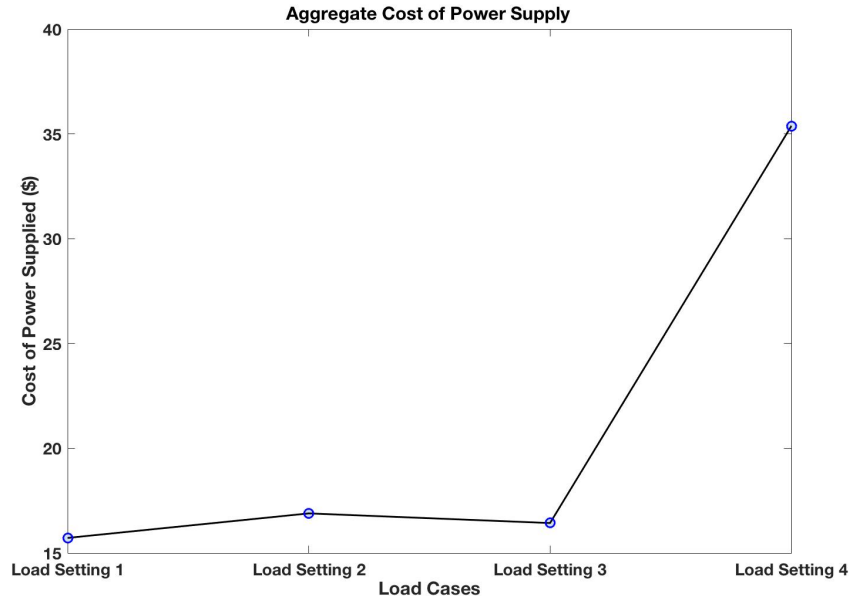
Figure 3.9: Optimal power cost in different load scenarios

to 1 while the cost of the other sources α_c are kept fixed to 100. Under these cost scenarios, the maximum deviation in the bus voltage magnitudes using the aforementioned incremental-cost based algorithm is shown in Fig. 3.10. These values were obtained by conducting Newton-Ralphson AC load flow analysis using MATPOWER function 'runpf' [62]. When the cost factor of source at 33 is biased to be 100 times less than the cost factors of other sources, the entire real power demand in the distribution system is being met by the source at 33. This results in significant voltage drop in the lines which causes the voltage magnitude deviation to surpass the allowed limit of 10%, where the maximum voltage in the system is considered to be 1.05 p.u. On the other hand, the optimization technique proposed in this paper accurately incorporates constraints related to line losses, voltage drops, reactive power balance and voltage feasibility limits. This prevents the proposed algorithm to limit the power drawn from source 33 and allocate some injection to the other sources so that the bus voltage limits are not violated. The results are shown in Fig. 3.10 where it can be seen that even for a highly biased cost, the proposed algorithm obtains a solution within standard voltage bounds, whilst optimization schemes ignoring essential constraints might violate these bounds.
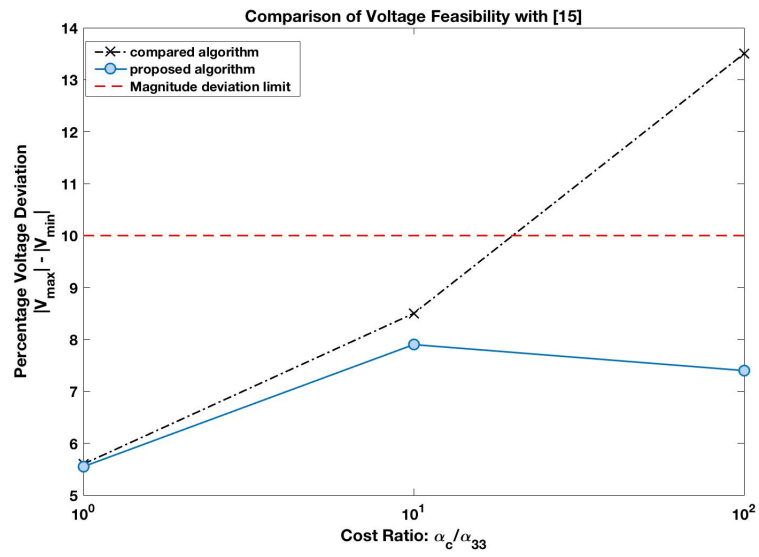
Figure 3.10: Comparison of voltage feasibility of final solution

Chapter 4

Conclusions

A paradigm shift in our energy landscape is being brought about by rapid development of the microgrid technology, which offers a reliable solution to modern energy needs and enables growing amalgamation of greener sources to our grid. Superior ability to monitor and engage in interactive energy exchange via demand side smart devices presents a unique opportunity to now control all significant entities in the power network. However, the full potential of this technology is yet to be realized due to lack of a comprehensive framework that can support a wide range of operational scenarios encountered in the microgrid. The imminent need to improve existing techniques to match the faster dynamics of microgrid elements and establish a more feasible, reliable and efficient scheme of coordinating distributed sources had been addressed through this work.

Utilities can use the proposed coordination schemes on microgrid systems with loads that can be controlled in short term (about a minute) to economize power supply costs from the distributed sources. The coordination scheme is foreseen to work in tandem with a transient control mechanism that deals with initial oscillations and abrupt changes in load within a coordination interval. The applicability of the individual techniques depend on the characteristics of the system loads and logistic limitations (e.g. computational power of bus agents).

4.1 Contributions

In light of the existing research challenges, the contributions of this thesis can be summarized as follows:

- Decentralization of the microgrid steady-state source coordination problem was achieved through application of ADMM that improves the reliability and scalability of centralized dispatch mechanisms by eliminating dependence on single point of failure.

- A source coordination technique incurring minimal computational cost is proposed by performing strategic linearization and convexification on a constant-impedance load modelled microgrid system that delivers feasible minimum-cost solutions for load compositions of reasonable power factors.

- A near real-time coordination technique of inverter based DERs is proposed that improves the previous method with an exact relaxation of the non-convex constraint in DQ frame state-space model of microgrid system. This technique is particularly well suited for islanded microgrids and guarantees feasibility of acquired solution for a wider range of load compositions.

- For grid-connected microgrids or active radial distribution networks, a novel method of solving BFM based OPF problem is presented that guarantees feasibility of quadratic equality constraint of line flow, which has not been achieved in existing formulations.

- Performance and key characteristics of all algorithms were exhibited through application on realistic microgrid parameters and detailed analysis.

4.2 Future work

This thesis work explores decentralized steady-state optimization of stand-alone microgrids and predominantly grid-connected microgrids considering the various operational constraints presented by standard operation of the network. Through appropriate relaxations, tractable and

scalable problems were developed that acquires solutions to the minimization problem while strictly maintaining the real-reactive power balances and imposing quality bounds (e.g. voltage deviation). Some future scopes of this research will entail:

- A transient source control mechanism that can work in tandem with the DQ based steady-state source dispatch model of the islanded microgrid. It will be designed to dynamically change the input parameters to compensate for abrupt or unexpected changes in micro-grid parameters between two coordination events.

- A more unified steady-state optimization problem that accounts for all different load types namely, constant-impedance, constant-current and constant-power (ZIP) models accurately in the problem constraints.

- A method to optimize the dual variable step size, ρ to achieve perfect balance between speed and accuracy of the decentralized coordination process. Some recent work in this area are using machine learning techniques to decide ρ depending on the system size and length of the variable set.

- A reformed problem formulation that can appropriately model unbalanced systems and incorporate non-controllable DERs that output set power using maximum power point tracking or other control mechanisms.

Bibliography

[1] M. Soshinskaya, W. H. Crijns-Graus, J.M. Guerrero and J.C. Vasquez, "Microgrids: Experiences, barriers and success factors," *Renewable and Sustainable Energy Reviews*, vol. 40, pp. 659-672, Dec. 2014

[2] R. L. Dohn "The business case for microgrids. White paper: The new face of energy modernization," Siemens AG, 2011. [Online]. Available: https://w3.usa.siemens.com/smartgrid/us/en/microgrid/Documents/The

[3] X. Lu, J. Wang, "A Game Changer: Electrifying Remote Communities by Using Isolated Microgrids," *IEEE Electrification Magazine* , vol. 5, no.2, pp. 56-63, Jun. 2017

[4] F. Luo, Z. Dong, G. Liang, J. Murata, Z. Xu "A Distributed Electricity Trading System in Active Distribution Networks Based on Multi-Agent Coalition and Blockchain," *IEEE Transactions on Power Systems*, 2019. (Early Access)

[5] D. E. Olivares, A. Mehrizi-Sani, A.H. Etemadi, C. Cañizares, R. Iravani, M. Kazerani, A.H. Hajimiragha, O. Gomis-Bellmunt, M. Saeedifard, R. Palma-Behnke *et al.*, "Trends in microgrid control," *IEEE Transactions on Smart Grid*, vol. 5, no. 4, pp. 1905-1919, Jul. 2014.

[6] J.M. Guerrero, J.C. Vasquez, J. Matas, L.G. de Vicuña, and M. Castilla, "Hierarchical control of droop-controlled AC and DC microgrids: A general approach toward standardization," *IEEE Transactions on Industrial Electronics*, vol. 58, no. 1, pp. 158-172, Jan. 2011.

[7] T.L. Vandoorn, J.D.M. De Kooning, B. Meersman, and L. Vandevelde, "Review of primary control strategies for islanded microgrids with power electronic interfaces," *Renewable and Sustainable Energy Reviews*, vol. 19, pp. 613-628, Mar. 2013.

[8] J. A. Taylor. *Convex Optimization of Power Systems*. Cambridge, UK: Cambridge University Press, 2015.

[9] M. Marzband, F. Azarinejadian, M. Savaghebi, and J.M. Guerrero, "An optimal energy management system for islanded microgrids based on multiperiod artificial bee colony combined with markov chain," *IEEE Systems Journal*, vol. 11, no. 3, pp. 1712-1722, Sep. 2017.

[10] L. Gan, N. Li, U. Topcu, S. Low "Branch flow model for radial networks: convex relaxation," in *Proc. of the 51st IEEE Conference on Decision and Control*, Piscataway, NJ, USA, 2012, pp. 1-8.

[11] P. P. Barker, R.W.D. Mello "Determining the impact of distributed generation on power systems. I. Radial distribution systems," in *Proc. of IEEE Power Engineering Summer Meeting*, vol. 3. Seattle, WA, USA, 2000, pp. 1645-1656.

[12] J.A.P Lopes, C.L. Moreira and A.G. Madureira, "Defining control strategies for microgrids islanded operation," *IEEE Transactions on Power Systems* , vol. 21, no. 2, pp. 916-924, May 2006

[13] A.H. Hajimiragha, M. R. Zadeh, "Research and development of a microgrid control and monitoring system for the remote community of Bella Coola: Challenges, solutions, achievements and lessons learned," in *Proc. of IEEE International Conference on Smart Energy Grid Engineering (SEGE)*, Oshawa, ON, Canada, Aug. 2013, pp. 1-6.

[14] R. P. Behnke, C. Benavides, F. Lanas, B. Severino, L. Reyes, J. Llanos, D. Sáez, "A microgrid energy management system based on the rolling horizon strategy," *IEEE Transactions on Smart Grid* , vol. 4, no. 2, pp. 996-1006, Jan. 2013

[15] S. S. Soman, H. Zareipour, O. Malik and P. Mandal, "A review of wind power and wind speed forecasting methods with different time horizons," in *Proc. of IEEE North American Power Symposium*, Arlington, TX, USA, Sep. 2010.

[16] F. Chen, M. Chen, Q. Li, K. Meng, and Y. Zheng, J.M. Guerrero, and D. Abbott, "Cost-based droop schemes for economic dispatch in islanded microgrids," *IEEE Transactions on Smart Grid*, vol. 8, no. 1, pp. 63-74, Jan. 2017.

[17] Yinliang Xu, Zhicheng Li, "Distributed optimal resource management based on the consensus algorithm in a microgrid," *IEEE Transactions on Industrial Electronics*, vol. 62, no. 4, pp. 2584-2592, Apr. 2015.

[18] B. Zhang , A.Y. Lam, A.D. Garcia and D.Tse, "An optimal distributed method for voltage regulation in power distribution systems." *IEEE Transactions on Power Systems*, vol. 30, no. 4, pp. 1714-1726, Jul. 2015.

[19] Q. Peng and S.H. Low, "Distributed algorithm for optimal power flow on a radial network," in *Proc. of the 53rd IEEE Annual Conference on Decision and Control*, CA, USA, Dec. 2014, pp. 167-172.

[20] T. Erseghe, "Distributed optimal power flow using ADMM," *IEEE Transactions on Power System*, vol. 29, no. 5, pp. 2370-2380, Sep. 2014.

[21] E. Dallanese, H. Zhu, and G.B. Giannakis, "Distributed optimal power flow for smart microgrids," *IEEE Transactions on Smart Grid*, vol. 4, no. 3, pp. 1464-1475, Sep. 2013.

[22] P. Lin, C. Jin, J. Xiao, X. Li, D. Shi, Y. Tang and P. Wang, "A distributed control architecture for global system economic operation in autonomous hybrid AC/DC microgrids," *IEEE Transactions on Smart Grid*, vol. 10, no. 3, pp. 2603-2617, May 2019.

[23] P. Vergara, J. Rey, H. Shaker, J. Guerrero, B. J. Jorgensen and L. Silva, "Distributed strategy for optimal dispatch of unbalanced three-phase islanded microgrids," *IEEE Transactions on Smart Grid*, vol. 10, no. 3, pp. 3210-3225, May 2019.

[24] A.H. Etemadi, E.J. Davison, and R. Iravani, "A decentralized robust control strategy for multi-der microgrids-part II: Performance Evaluation," *IEEE Transactions on Power Delivery*, vol. 27, no. 4, pp. 1854-1861, Oct. 2012.

[25] A.H. Etemadi, E.J. Davison, and R. Iravani, "A decentralized robust control strategy for multi-der microgrids-part I: Fundamental concepts," *IEEE Transactions on Power Delivery*, vol. 27, no. 4, pp. 1843-1853, Oct. 2012.

[26] Q. Peng, S. Low "Distributed optimal power flow algorithm for balanced radial distribution networks," *arXiv preprint arXiv:1404.0700*, May 2015.

[27] L. Tao, C. Schwaegerl, S. Narayanan, J.H. Zhang "From laboratory Microgrid to real markets: Challenges and opportunities," in *Proc. of 8th IEEE International Conference on Power Electronics-ECCE Asia*, Jeju, South Korea, 2011, pp. 264-271.

[28] D.L. Yao, S.S. Choi, K.J. Tseng and T.T. Lie "A statistical approach to the design of a dispatchable wind power-battery energy storage system," *IEEE Transactions on Energy Conversion*, vol. 24, no. 4, pp. 916-925, Dec. 2009

[29] R. Majumder; A. Ghosh; G. Ledwich; F. Zare, "Control of parallel converters for load sharing with seamless transfer between grid connected and islanded modes," in *Proc. of IEEE Power and Energy Society General Meeting*, Pittsburgh, PA, USA, Jul. 2008, pp. 1-7.

[30] GC Liao, JI Tsai "Use of a new method to solve the economic dispatch problem of smart microgrid including distributed generation," in *Proc. of Asia-Pacific Power and Energy Engineering Conference*, Shanghai, China, Mar. 2012, pp. 1-4.

[31] W.H. Kersting and W.H. Phillips, "Distribution feeder line models," in *Proc. of the 1994 IEEE Rural Electric Power Conference*, Colorado Springs, CO, USA, Apr. 1994.

[32] C.L. Masters, "Voltage rise: the big issue when connecting embedded generation to long 11 kV overhead lines," *IET Power Engineering journal*, vol. 16, no. 1, pp. 5-12, Feb. 2002.

[33] P. Krause; O. Wasynczuk, SD Sudhoff, S. Pekarek, *Analysis of Electric Machinery and Drive System* New York, USA: IEEE Press, 2002.

[34] A.G. Phadke, J. Thorp, *Synchronized Phasor Measurements and Their Applications*, 1st ed. New York, USA: Springer, 2008.

[35] *IEEE Standard for Synchrophasors for Power Systems*, IEEE Standard C37.118-2005, 2006, (Revision of IEEE Standard 1344-1995).

[36] Pennsylvania State University. The phase plane portraits of linear systems. Available: http://www.math.psu.edu/tseng/class/Math251/Notes-PhasePlane.pdf

[37] H. Farhangi, "The path of the smart grid," *IEEE Power Energy Magazine*, vol. 8, no. 1, pp. 18-28, Jan./Feb. 2010

[38] S.C. Ergen. (2004). ZigBee/IEEE 802.15. 4 Summary. [Online]. Available: http://pages.cs.wisc.edu/ suman/courses/707/papers/zigbee.pdf

[39] B. Krupanek and R. Bogacz, *Investigations of transmission delays in ZigBee networks*, Politechnika Slaska, Instytut Metrologii, Elektroniki i Automatyki, vol. 1, no. 2, 2014.

[40] M. Ross, C. Abbey, F. Bouffard, and G. Jos, "Multiobjective optimization dispatch for microgrids with a high penetration of renewable generation," *IEEE Transaction on Sustainable Energy*, vol. 6, no. 4, pp. 1306-1314, Oct. 2015.

[41] *Electric Power Systems and Equipment-Voltage Ratings (60 Hz)*, ANSI Std. C84.1, 2016

[42] S. Boyd and L. Vandenberghe. *Convex Optimization* . Cambridge, UK: Cambridge university press, 2004.

[43] S. Boyd, N. Parikh, E. Chu, B. Peleato, and J. Eckstein, "Distributed optimization and statistical learning via the alternating direction method of multipliers," *Foundations and Trends in Machine Learning*, vol. 3, no. 1, pp. 1-122, July 2011.

[44] C. Coffrin, P. V. Hentenryck, "A linear-programming approximation of AC power flows," *INFORMS Journal on Computing*, vol. 26, no.4, pp. 718-734, May 2014.

[45] C.S. Cheng and D. Shirmohammadi "A three-phase power flow method for real-time distribution system analysis," *IEEE Transactions on Power Systems*, vol. 10, no. 2, pp. 671-679, May 1995.

[46] *IEEE Guide for Design, Operation, and Integration of Distributed Resource Island Systems with Electric Power Systems*, IEEE Standard 1547.4, Jul. 2011.

[47] F. Bell, A. Nguyen, M. McCarty, K. Atef, and T. Bialek, "Secondary voltage and reactive power support via smart inverters on a high-penetration distributed photovoltaic circuit," in *Proc. of the IEEE Power & Energy Society Innovative Smart Grid Technologies Conference (ISGT)*, Minneapolis, MN, USA, 2016, pp. 1-6.

[48] G.P. Adam, O.A. Lara, G.M. Burt, D. Telford, B.W. Williams, and J.R. McDonald, "Modular multilevel inverter: Pulse width modulation and capacitor balancing technique," *IET Power Electronics*, vol. 3, no. 5, pp. 702-715, Sept. 2010.

[49] R. Reginatto and R. A. Ramos, "On electrical power evaluation in dq coordinates under sinusoidal unbalanced conditions," *IET Generation, Transmission & Distribution*, vol. 8, no. 5, pp. 976-982, May 2014.

[50] H. Lotfi and A. Khodaei, "AC versus DC microgrid planning," *IEEE Transactions on Smart Grid*, vol. 8, no. 1, pp. 296-304, Jan. 2017.

[51] Y. Singer. (2014). Advanced optimization: Lecture-10. [Online]. Available: http://people.seas.harvard.edu/ yaron/AM221/lecturenotes/AM221lecture10.pdf

[52] D.E. Douglas and E.V. Heynsworth, "An identity for the Schur complement of a matrix," *Proceedings of the American Mathematical Society*, vol. 22, no. 2, pp. 364-366, Aug. 1969.

[53] J. Park, S. Boyd "General heuristics for nonconvex quadratically constrained quadratic programming," *arXiv preprint arXiv:1703.07870*, May 2017.

[54] S. Low "Convex relaxation of optimal power flow-Part I: Formulations and equivalence," *IEEE Transactions on Control of Network Systems*, vol. 1, no. 1, pp. 15-27, Mar. 2014.

[55] M. Farviar, S. Low "Branch flow model: Relaxations and convexification-Part I," *IEEE Transactions on Power Systems*, vol. 28, no. 3, pp. 2554-2564, Aug. 2013.

[56] M. Baran, F. Wu "Optimal capacitor placement on radial distribution systems," *IEEE Transactions on Power Delivery*, vol. 4, no. 1, pp. 725-734, Jan. 1989.

[57] M. Baran, F. Wu "Optimal sizing of capacitors placed on a radial distribution system," *IEEE Transactions on Power Delivery*, vol. 4, no. 1, pp. 735-743, Jan. 1989.

[58] J. Beerten, S. Cole, R. Belmas "Generalized steady-state VSC MTDC model for sequential AC/DC power flow algorithms," *IEEE Transactions on Power Systems*, vol. 27, no. 2, pp. 821-829, May 2012.

[59] S. Huang, Q. Wu, J. Wang, H. Zhao, "A sufficient condition on convex relaxation of AC optimal power flow in distribution networks," *IEEE Transactions on Power Systems*, vol. 32, no. 2, pp. 1359-1368, Mar. 2017.

[60] G. Meurant, *Algorithms and Complexity*. Amsterdam, The Netherlands: Elsevier, 1990.

[61] P. Srikantha, D. Kundur "Hierarchical Signal Processing for Tractable Power Flow Management in Electric Grid Networks," *IEEE Transactions on Signal and Information Processing over Networks*, vol. 5, no. 1, pp. 86-99, Jul. 2018.

[62] R. D. Zimmerman, S. Murillo, E. Carlos, R.J. Thomas, "MATPOWER: Steady-state operations, planning, and analysis tools for power systems research and education," *IEEE Transactions on power systems*, vol. 26, no. 1, pp. 12-19, Jun. 2010.

[63] M.E. Baran, F. F. Wu, "Network reconfiguration in distribution systems for loss reduction and load balancing," *IEEE Transactions on power delivery*, vol. 4, no. 2, pp. 1401-1407, Apr. 1989.

Appendix A

Proof of Theorem on ρ bound

In this section, we will outline the mathematical proof of deriving the expression in Theorem 2.5.1 which ensures the convexity of the objective function of ADMM subproblem $\mathcal{P}_{U1}$. The objective of the subproblem is:

$$f_i(x_i) = x_i^T \left(A_0^i + B_0^i \right) x_i + C_0^i x_i$$

The quadratic terms associated with variables $\{V_i, V_{ti}\}$ in the objective introduces the non-convexity in the cost function. Hence, we specifically show the matrix segment associated with these variables below:

$$f_i \left(V_{i,dq}, V_{ti,dq} \right) = \begin{bmatrix} V_{i,dq} & V_{ti,dq} \end{bmatrix}^T (A_{S0}^i + B_{S0}^i) \begin{bmatrix} V_{i,dq} & V_{ti,dq} \end{bmatrix}$$

$$\text{where } A_{S0}^i = \frac{\frac{3}{2} K_i}{R_{fi}^2 + (\omega L_{fi})^2} \begin{bmatrix} 0 & 0 & -\frac{R_{fi}}{2} & \frac{\omega L_{fi}}{2} \\ 0 & 0 & -\frac{\omega L_{fi}}{2} & -\frac{R_{fi}}{2} \\ -\frac{R_{fi}}{2} & -\frac{\omega L_{fi}}{2} & R_{fi} & 0 \\ \frac{\omega L_{fi}}{2} & -\frac{R_{fi}}{2} & 0 & R_{fi} \end{bmatrix}$$

$$\text{and } \left(B_{S0}^i \right)_{\text{worst case}} = 2 diag(\rho, \rho, \rho, \rho)$$

The worst case $(B_{S0})^i$ considered arises for starting bus in the configuration, because it does not have the consensus contraint associated with preceding bus voltage, V_{i-1}^x. For all other buses, the first two diagonal elements $(B_{S0})^i$ is 2ρ. For the ρ limit to be applicable to all buses in the network, we consider the worst case $(B_{So})^i$ for all subsequent calculations. The convexity of the objective is dependent on the positive semi-definiteness of the sum of quadratic coefficient matrices [42] i.e. (i.e. $(A_{S0}^i + B_{S0}^i) \succeq 0$) which can be expanded as:

$$
\begin{bmatrix}
\rho & 0 & -\frac{a-\rho}{2} & \frac{b}{2} \\
0 & \rho & -\frac{b}{2} & -\frac{a-\rho}{2} \\
-\frac{a-\rho}{2} & -\frac{b}{2} & a & 0 \\
\frac{b}{2} & -\frac{a-\rho}{2} & 0 & a
\end{bmatrix} \succeq 0 \quad \text{where,}
$$

$$
a = \rho + R_{fi} \cdot \frac{\frac{3}{2} K_i}{R_{fi}^2 + (\omega L_{fi})^2}, \quad b = \omega L_{fi} \cdot \frac{\frac{3}{2} K_i}{R_{fi}^2 + (\omega L_{fi})^2}
$$

To determine the range of ρ for which the eigenvalues, e of the above matrix is positive, the characteristic equation associated with the matrix: $det(A_0^i + B_0^i - \mathbf{I}e) = 0$ has been solved. This leads to the following expression after certain algebraic manipulations:

$$
\left[(\rho - e)(a - e) - \frac{(a-\rho)^2}{4} - \frac{b^2}{4} \right]^2 = 0
$$

Solving the above equation for e will clearly result in two sets of repeated roots of the characteristic equation where each of them can be evaluated as:

$$
e_{repeated} = \frac{(a + \rho) \pm \sqrt{(a+\rho)^2 - 4\{a\rho - \frac{(a-\rho)^2}{4} - \frac{b^2}{4}\}}}{2}
$$

For the matrix $(A_0^i + B_0^i)$ to be PSD, it is sufficient to set the non-negativity condition on the

smaller of the two eigenvalues that are obtained using the characteristic equation that is:

$$\frac{(a + \rho) - \sqrt{(a + \rho)^2 - 4\{a\rho - \frac{(a-\rho)^2}{4} - \frac{b^2}{4}\}}}{2} \geq 0$$

Finally, substituting the expressions for a and b in the above equation, the lower limit of ρ in terms of the microgrid parameters can be shown as:

$$\rho \geq \sqrt{\frac{1}{2}\left(R_{fi} \cdot \frac{\frac{3}{2}K_i}{R_{fi}^2 + (\omega L_{fi})^2}\right)^2 + \frac{1}{4}\left(\omega L_{fi} \cdot \frac{\frac{3}{2}K_i}{R_{fi}^2 + (\omega L_{fi})^2}\right)^2} - \frac{1}{2}\left(R_{fi} \cdot \frac{\frac{3}{2}K_i}{R_{fi}^2 + (\omega L_{fi})^2}\right)$$

Setting D_i to be $\frac{2}{3}(R_{fi}^2 + (\omega L_{fi})^2)$, the final expression shown in Theorem 2.5.1 is obtained.

Appendix B

Parameters for Studies in Chapter 2

DER		X-er		Load	
$S_{rating1}$	1.6 MVA	X_{T1}	0.08p.u.	R_1	2.94 p.u.
R_{f1}	0.0046 p.u.			R_{l1}	0.02 p.u.
L_{f1}	0.23 p.u.			X_{l1}	0.35 p.u.
				X_{C1}	0.37p.u.

Table B.1: Parameters of Bus Type 1

DER		X-er		Load	
$S_{rating2}$	1.6 MVA	X_{T2}	0.08p.u.	R_2	3.15 p.u.
R_{f2}	0.0046 p.u.			R_{l2}	0.02 p.u.
L_{f2}	0.23 p.u.			X_{l2}	0.32 p.u.
				X_{C2}	0.34p.u.

Table B.2: Parameters of Bus Type 2

DER		X-er		Load	
$S_{rating3}$	1.6 MVA	X_{T3}	0.08p.u.	R_3	3.36 p.u.
R_{f3}	0.0046 p.u.			R_{l3}	0.02 p.u.
L_{f3}	0.23 p.u.			X_{l3}	0.38 p.u.
				X_{C3}	0.41p.u.

Table B.3: Parameters of Bus Type 3

Line Impedance	
R_{t1}	0.0145 p.u.
X_{t1}	0.013 p.u.

Table B.4: For line between bus type $1 \to 2$

Line Impedance	
R_{t2}	0.029 p.u.
X_{t2}	0.026 p.u.

Table B.5: For line between bus type $2 \to 3$

Bus position	Bus type	Bus position	Bus type
1	Type 1	16	Type 3
2	Type 2	17	Type 1
3	Type 3	18	Type 3
4	Type 2	19	Type 1
5	Type 1	20	Type 3
6	Type 3	21	Type 1
7	Type 1	22	Type 2
8	Type 3	23	Type 3
9	Type 1	24	Type 2
10	Type 3	25	Type 1
11	Type 1	26	Type 3
12	Type 2	27	Type 1
13	Type 3	28	Type 3
14	Type 2	29	Type 1
15	Type 1	30	Type 3

Table B.6: Configuration of 30-bus system

Appendix C

Parameters for Studies in Chapter 3

Table C.1: Real and Reactive Generation Capacity of DGs

Source on Bus	$P_{G,min}(MW)$	$P_{G,max}(MW)$	$Q_{G,min}(MVar)$	$Q_{G,max}(MVar)$
1	-	-	-	-
6	0	5	-3	3
20	0	3	-2	2
33	0	3	-2	2

Table C.2: Combinations of cost factor α utilized for simulations Fig. 3.5

Source on Bus	1	6	20	33
Cost Combo 1	1	8	8	8
Cost Combo 2	8	1	8	8
Cost Combo 3	8	8	1	8
Cost Combo 4	8	8	8	1
Cost Combo 5	8	8	8	8

Table C.3: Different Load Settings of IEEE 33-bus system utilized for simulations Fig. 3.6-3.9

Bus No.	Load Setting 1		Load Setting 2		Load Setting 3	
	$P_L(MW)$	$Q_L(MVar)$	$P_L(MW)$	$Q_L(MVar)$	$P_L(MW)$	$Q_L(MVar)$
1	-	-	-	-	-	-
2	0.10	0.06	0.10	0.06	0.10	0.09
3	0.09	0.04	0.09	0.04	0.09	0.06
4	0.12	0.08	0.12	0.08	0.12	0.12
5	0.06	0.03	0.06	0.03	0.06	0.045
6	0.06	0.02	0.06	0.02	0.06	0.03
7	0.20	0.10	0.20	0.10	0.20	0.15
8	0.20	0.10	0.20	0.10	0.20	0.15
9	0.06	0.02	0.61	0.02	0.06	0.03
10	0.06	0.02	0.06	0.02	0.06	0.03
11	0.045	0.03	0.045	0.03	0.045	0.045
12	0.06	0.035	0.06	0.035	0.06	0.053
13	0.06	0.035	0.06	0.035	0.06	0.053
14	0.12	0.08	0.06	0.08	0.12	0.12
15	0.06	0.01	0.06	0.01	0.06	0.015
16	0.06	0.02	0.06	0.02	0.06	0.03
17	0.06	0.02	0.06	0.02	0.06	0.03
18	0.09	0.04	0.09	0.04	0.09	0.06
19	0.09	0.04	0.09	0.04	0.09	0.06
20	0.09	0.04	0.09	0.04	0.09	0.06
21	0.09	0.04	0.09	0.04	0.09	0.06
22	0.09	0.04	0.09	0.04	0.09	0.06
23	0.09	0.05	0.09	0.05	0.09	0.075
24	0.42	0.20	0.42	0.20	0.42	0.30
25	0.42	0.20	0.22	0.20	0.42	0.30
26	0.06	0.025	0.06	0.025	0.06	0.038
27	0.06	0.025	0.06	0.025	0.06	0.038
28	0.06	0.02	0.06	0.02	0.06	0.03
29	0.12	0.07	0.06	0.07	0.12	0.105
30	0.20	0.60	0.10	0.60	0.20	0.90
31	0.15	0.07	0.10	0.07	0.15	0.105
32	0.21	0.10	0.13	0.10	0.21	0.15
33	0.06	0.04	0.06	0.04	0.06	0.06

Bus No.	Load Setting 4	
	$P_L(MW)$	$Q_L(MVar)$
1	-	-
2	0.20	0.09
3	0.18	0.06
4	0.24	0.12
5	0.12	0.045
6	0.12	0.03
7	0.40	0.15
8	0.40	0.15
9	0.12	0.03
10	0.12	0.03
11	0.09	0.045
12	0.12	0.053
13	0.12	0.053
14	0.24	0.12
15	0.12	0.015
16	0.12	0.03
17	0.12	0.03
18	0.18	0.06
19	0.18	0.06
20	0.18	0.06
21	0.18	0.06
22	0.18	0.06
23	0.18	0.075
24	0.84	0.30
25	0.84	0.30
26	0.12	0.038
27	0.12	0.038
28	0.12	0.03
29	0.24	0.105
30	0.40	0.90
31	0.30	0.105
32	0.42	0.15
33	0.12	0.06

Curriculum Vitae

Name:	Mithun Mallick
Post-Secondary Education and Degrees:	Bangladesh University of Engineering & Technology Dhaka, Bangladesh 2013-2017 (B. Sc.) University of Western Ontario London, ON 2017 - 2019 M. E. Sc.
Related Work Experience:	Teaching Assistant Western University 2017 - 2019 Research Assistant Western University 2017-2019

Publications:

- M. Mallick, P. Srikantha, "Optimal Decentralized Microgrid Coordination via the Schur's Complement and S-Procedure," IEEE Transactions on Smart Grid, 2019. (Early Access)

- M. Mallick, P. Srikantha, "Optimal Decentralized Coordination of Voltage-Controlled Sources in Islanded Microgrids," 2018 IEEE International Conference on Communications, Control, and Computing Technologies for Smart Grids (SmartGridComm), Aalborg, Denmark.